Dynamics of particle settling and resuspension in viscous liquid films

N. Murisic[1] †, B. Pausader[2], D. Peschka[3], A.L. Bertozzi[1]

[1] Department of Mathematics, University of California, Los Angeles, 520 Portola Plaza, Los Angeles, California 90095, USA

[2] Courant Institute of Mathematical Sciences, New York University, 251 Mercer Street, New York , New York 10012, USA

[3] Weierstrass-Institute for Applied Analysis and Stochastics, Mohrenstr. 39, 10117 Berlin, Germany

(Received 28 September 2012)

We develop a dynamic model for suspensions of negatively buoyant particles on an incline. Our model includes settling due to gravity and resuspension of particles by shear-induced migration. We consider the case where the particles settle onto the solid substrate and two distinct fronts form – a faster liquid and a slower particle front. The resulting transport equations for the liquid and the particles are of hyperbolic type and we study the dilute limit for which we compute exact solutions. We also carry out systematic laboratory experiments, focusing on the motion of the two fronts. We show that the dynamic model predictions for small to moderate values of the particle volume fraction and the inclination angle of the solid substrate agree well with the experimental data.

1. Introduction and Background

Despite their relevance in industrial and environmental applications, the systems involving settling and resuspension of particles in viscous liquids are still not fully understood. The seminal works on this subject, e.g. Kynch (1952), Richardson & Zaki (1954), Leighton & Acrivos (1987*b*), Schaflinger *et al.* (1990), Acrivos *et al.* (1992), and Nott & Brady (1994), have primarily focused on sedimentation in quiescent liquid medium, Couette or channel flows. A review of developments in sedimentation of mono- and polydisperse suspensions, and in inclined channels was given in Davis & Acrivos (1985). Our focus in this paper is on particle-laden thin-film flows on an incline, involving a free surface and contact lines. Due to complexities resulting from a perplexing interplay of relevant mechanisms, including settling/resuspension and viscous fingering at the contact line, only recent studies have begun to address this class of problems, e.g. Zhou *et al.* (2005) and Cook (2008). While particle-laden thin-film flows represent a formidable problem from the theoretical standpoint, these flows are captured through relatively simple experiments, see e.g. Ward *et al.* (2009) and Murisic *et al.* (2011).

When a rigid spherical particle settles under the influence of gravity through an unbounded quiescent liquid, the well-known Stokes' law applies. Namely, the settling velocity of the particle is $U_{\mathrm{St}} = d^2(\rho_p - \rho_l)g/(18\mu_\ell)$, where d is the particle diameter, ρ_p and ρ_ℓ are particle and liquid mass densities respectively, g is the magnitude of the gravitational acceleration, and μ_ℓ is the liquid viscosity. When many such particles settle, the Stokes' law is modified and the average settling velocity of a particle is $U_{\mathrm{St}}\Phi(\phi)$. The hindrance

† Present address: Lewis-Sigler Institute for Integrative Genomics, Princeton University, Princeton, New Jersey 08544, USA

function $\Phi(\phi)$ accounts for particle-particle interaction where ϕ is the particle volume fraction, such that $\Phi(0) = 1$. This type of hindrance was first studied in Richardson & Zaki (1954), where $\Phi(\phi) = (1-\phi)^m$ with $m \approx 5.1$ was constructed empirically. Alternate forms of $\Phi(\phi)$ have since been proposed, e.g. for dilute dispersions in Batchelor (1972), or $\Phi(\phi) = (1-\phi)$ in the presence of shear, see Schaflinger *et al.* (1990).

A review by Stickel & Powell (2005) focused on the rheology of dense suspensions. They concluded that in highly concentrated suspensions, multi-body interactions and two-body lubrication are relevant, and non-Newtonian rheology should be considered. Their dimensional analysis indicated that, given the values of d, ρ_ℓ and μ_ℓ, the suspension is expected to behave like a Newtonian fluid for a relatively narrow range of shear rates. This range was found to widen as d and μ_ℓ were increased. They also discussed the related issue of the effective suspension viscosity and reviewed several commonly used models.

Experiments with concentrated suspensions in Couette flows showed that heavy particles need not settle when shear is present. This and other interesting phenomena occurring in a suspension flow in a Couette viscometer were first studied by Leighton & Acrivos (1987*a*). Their observations were attributed to a novel mechanism they called shear-induced migration. Shear-induced migration has since been studied in various flow geometries. There have been two distinct approaches to modeling shear-induced migration and both have been successful in capturing experimental observations.

The first approach, which is used here, relies on a diffusive flux phenomenology. It was first formulated in Leighton & Acrivos (1987*b*) in order to model the experimental observations from Leighton & Acrivos (1987*a*). It was based on irreversible interactions between pairs of particles, whereby the particles migrate via a diffusive flux induced by gradients in both ϕ and the effective suspension viscosity, $\mu(\phi)$. A similar but somewhat simplified approach was later used for modeling suspensions of heavy particles in pressure-driven channel flows by Schaflinger *et al.* (1990). The model from Leighton & Acrivos (1987*b*) was further refined by Phillips *et al.* (1992) who applied it to a flow of a neutrally-buoyant suspension in a Couette device. This approach was also used for laminar pipe flows in Zhang & Acrivos (1994), and for rotating parallel-plate flows in Merhi *et al.* (2005). More recently, the diffusive flux phenomenology was utilized in modeling thin-film flows of negatively-buoyant suspensions in Cook (2008) and Murisic *et al.* (2011), successfully capturing experimental observations. In particular, the model predictions in Murisic *et al.* (2011) were in excellent agreement with the phase separation diagrams resulting from experiments where both d and μ_ℓ were varied.

The second approach was developed by Nott & Brady (1994) and it is known as the suspension balance approach. It was originally derived to model pressure-driven rectilinear suspension flows. The two approaches differ in two significant aspects. The first has to do with the rheological model that is used; the second is related to the manner in which particle migration is included. In the diffusive flux approach, a Newtonian viscosity depends only on the particle volume fraction, ϕ, while the particle flux expression is empirical. The suspension balance approach relies on a non-Newtonian bulk stress with normal stresses induced by shear; particle migration is caused by gradients in the normal stress. Hence, viscously generated normal stresses are present in the suspension balance approach and have a very important role. In contrast, they are omitted in the diffusive flux approach. Numerical simulations of models based on the suspension balance approach were carried out using the Stokesian Dynamics framework, e.g. see Nott & Brady (1994). Subsequent works employed this approach to particle-laden channel flows and curvilinear flows, see Brady & Morris (1997), Morris & Brady (1998), Morris & Boulay (1999) and Timberlake & Morris (2005). For example, a pressure driven flow of a dense suspension was studied in Morris & Brady (1998). Their numerical simulations revealed an equilibrium distribution with the heavier material on top of the lighter, providing a mechanical basis for maintaining the normal stresses in their migration model.

The suspension studies so far have mainly focused on Couette or channel flows. Only more recent works have concentrated on the problem of particle-laden thin-film flows on an incline. In Zhou *et al.* (2005), experiments with suspensions of glass beads, $d \sim \mathcal{O}(100\mu m)$, were carried out. The bulk particle volume fraction, ϕ_0, and the inclination angle, α, were varied and, depending on the values of these parameters, three different regimes were observed. When ϕ_0 and α were small, the *settled* regime resulted, where the particles settled out of the flow and the clear liquid flowed over the particulate bed. Two distinct fronts formed in this regime, a particle front and a clear liquid front. The latter was faster and it was susceptible to the well-known fingering instability, typical for clear liquid films. For large values of ϕ_0 and α, the *ridged* regime was observed, where the particles flowed faster than the liquid phase, accumulating at the front of the flow and eventually forming a ridge at the contact line. Finally, for intermediate values of ϕ_0 and α, the suspension remained *well-mixed* throughout the experiment. Their theoretical model was based on the Navier-Stokes equations for the liquid and a continuum diffusive model for the particles, including hindered settling. It was simplified by neglecting the capillary terms, and studied using a shock-dynamics approach, a direction further pursued in Cook *et al.* (2007). The model was successful at describing the details of the ridged regime. Shear-induced migration was first included in modeling particle-laden thin-film flows in Cook (2008). In this work, an equilibrium model was derived, based on the balance of hindered settling and shear-induced migration. Its predictions agreed well with the experimental data from Zhou *et al.* (2005), capturing transitions from the well-mixed state. In Ward *et al.* (2009), particle-laden thin-film flows on an incline were studied experimentally, concentrating on the front propagation in the well-mixed and ridged regimes for both heavy and light particles. The front position was found to obey a power law in time t with an exponent close to the well-known value 1/3 from Huppert (1982). In Grunewald *et al.* (2010), the self-similarity in a lubrication-based model for the case of constant volume flows was explored, with the main focus on the ridged regime. In Murisic *et al.* (2011), extensive experiments were carried out and the influence of the particle size and the viscosity of the suspending liquid were examined. The experiments confirmed the transient nature of the well-mixed regime. An extension of the equilibrium model from Cook (2008) was employed, and a time-scales argument was introduced, explaining the dynamics of the transition between the well-mixed and settled regimes. A dynamic model for particle-laden thin-film flows was also introduced, based on a coupled set of hyperbolic conservation laws. In Mata & Bertozzi (2011), a model similar to Zhou *et al.* (2005) but including capillarity was solved using a novel numerical approach.

In this paper, we systematically derive a dynamic model for particle and liquid transport in order to better understand the less-studied *settled* regime. For this purpose, we carry out both theoretical and experimental work. We study a suspension flow on an incline, having a constant volume and consisting of negatively buoyant particles with uniform size in a viscous suspending liquid. In this regime, gravity drives the flow down the incline and leads to a stratification of the suspension. We consider a continuum model, including the effects of hindered settling and shear-induced migration. The model is based on the Stokes' equations for an incompressible variable viscosity suspension, and the conservation of total mass of particles. The effect of shear-induced migration is included via the diffusive flux phenomenology. A dynamic model for transport of liquid and particles is developed using an asymptotic approach. Due to the disparity in the relevant time-scales, a fast one for the settling and a slow one for the suspension flow, we are able to assume that the particle distribution is in equilibrium along the direction

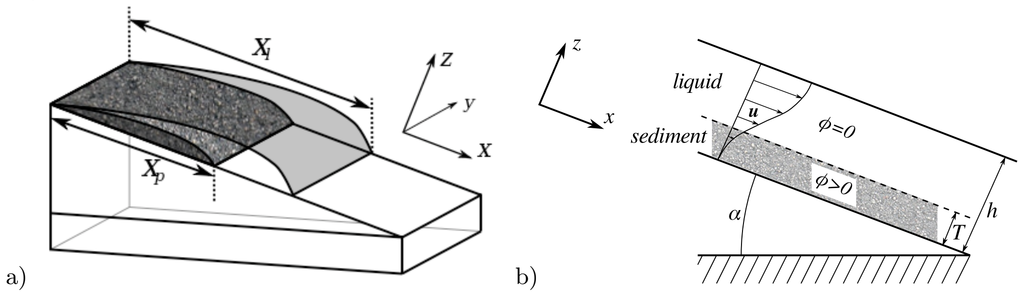

FIGURE 1. Sketches of the setup: a) the flow of a suspension film on an incline showing the sediment layer, and the two fronts; and b) a cross-section detail.

normal to the solid substrate (the settling direction) while the particles are transported along the solid substrate (the flow direction). Hence, we formally connect the equilibrium model with the dynamic one in a single framework. We explicitly confirm the hyperbolicity of the dynamic model and consider the dilute limit for which we derive the analytic solution. We also study the settled regime experimentally by carrying out extensive experiments where the bulk particle volume fraction and the inclination angle are varied over a wide range of values. In these experiments, we focus on the evolution of the two fronts, the particle and the liquid one. Finally, we solve the hyperbolic conservation laws numerically and compare the model predictions with the experiments.

The paper is organized as follows. In §2, we introduce the model and show how the lubrication approximation may be employed to find advection equations for suspension volume and particle volume fraction. We also explain how the details of the model depend on the bulk particle volume fraction and the inclination angle. In §3, we describe the experimental observations. Next, in §4, we solve the dynamic model numerically and compare its predictions with the experiments. We conclude with a brief discussion.

2. Theory

We consider a thin-film flow of a finite volume suspension consisting of a viscous liquid and spherical monodisperse non-colloidal negatively buoyant particles. The particles are assumed to be rigid and the liquid is incompressible. The modeling is carried out within the continuum limit. The flows are assumed to obey the transverse (y-direction) symmetry, see Fig. 1a); therefore, the cross-section of the flow is considered throughout the paper. Henceforth, we use the subscripts p and ℓ to differentiate between quantities corresponding to the particles and the suspending liquid respectively. Since the particles are heavy, the mass densities satisfy $\rho_p > \rho_\ell$.

Figure 1 shows the setup. The x- and z-coordinates are in the directions along and normal to the solid substrate respectively. The solid substrate is located at $z = 0$ and the inclination angle of the solid is α. The total suspension thickness is denoted by $h(x,t)$. Our focus is on the *settled* regime for which a dense sedimentation layer of particles forms close to the solid substrate, the region $0 \le z \le T$ where $T < h$, with a clear liquid layer ($\phi = 0$) on top of it, $T < z \le h$. At each time t and point (x,z), the particle volume fraction, $0 \le \phi(t,x,z) < 1$, and the volume-averaged velocity, $\mathbf{u}(t,x,z) = (u(t,x,z), w(t,x,z))^\top$, are defined. The incompressibility assumption translates to $\nabla \cdot \mathbf{u} = 0$.

For monodisperse spheres, the upper bound for ϕ is less than unity. This bound corresponds to the maximum packing fraction, $\phi_{\rm m}$. A priori prediction of its value is still an open question since $\phi_{\rm m}$ depends on all the parameters that affect the microstructure of the suspension, see e.g. Stickel & Powell (2005). A range of values $[0.524, 0.740]$ for ϕ_{m} may be obtained depending on the details of the geometric arrangement of the spheres, see Torquato *et al.* (2000). A well-mixed suspension forms the so-called random close-packed arrangement; an approximation $\phi_{\mathrm{m}} \approx 0.63$ for this case was obtained experimentally by McGeary (1961). Here, we use $\phi_{\mathrm{m}} = 0.61$, obtained as follows: known volumes of liquid and particles are mixed and placed in a graduated cylindrical container; the ϕ_{m} value is estimated from the excess liquid volume fraction. This value is larger than 0.55 from Onoda & Liniger (1990), corresponding to random loose-packing.

We consider suspensions that satisfy the following conditions: i) the particle Reynolds number is negligibly small, $\mathrm{Re} = \rho_\ell d^2 \dot{\gamma}/(4\mu_\ell) \sim \mathcal{O}(10^{-5})$; and ii) the Péclet number is very large, $\mathrm{Pe} = \dot{\gamma} d^2/D \sim \mathcal{O}(10^{10})$. The shear rate $\dot{\gamma} \sim \mathcal{O}(10^{-1})\, s^{-1}$ is defined below; here, $\rho_\ell \sim \mathcal{O}(10^3)\, kg\, m^{-3}$, $d^2 \sim \mathcal{O}(10^{-7})\, m^2$ and $\mu_l \sim \mathcal{O}(1)\, kg\, m^{-1}\, s^{-1}$; also, $D = kT/(3\pi\mu_\ell d) \sim \mathcal{O}(10^{-18})\, m^2\, s^{-1}$ is the diffusivity and kT is the thermal energy of the suspending liquid. Under these conditions, the effective suspension viscosity may be assumed to depend on the particle volume fraction only, $\mu = \mu(\phi)$, i.e. the suspension behaves like a Newtonian fluid. Also, since $\mathrm{Pe}/\mathrm{Re} \gg 1$, this behavior is expected to persist for a wide range of shear rates, see Stickel & Powell (2005). Different forms of $\mu(\phi)$ have appeared in literature. Typically, $\mu(\phi)/\mu_\ell \to \infty$ as $\phi \to \phi_{\mathrm{m}}$ is required. The definition of $\mu(\phi)$ usually includes ϕ_{m} as a direct measure of the suspension microstructure, see Stickel & Powell (2005). The functional form for $\mu(\phi)$ that we use is given below.

We derive a reduced model where the local state can be uniquely characterized by average quantities. As a starting point, we consider the Stokes' equations for the suspension and a conservation law for particle volume. Our modeling approach relies on the standard lubrication approximation used for thin-film flows, e.g. see Oron *et al.* (1997). The key ingredient here is the careful scaling of the particle transport terms that allows the particle flux in the z-direction to vanish at the leading order. Asymptotically higher order terms in the particle volume conservation law together with the lubrication style balances for suspension volume and momentum provide a set of coupled partial differential equations for the suspension height and the depth-averaged particle concentration. This amounts to assuming that the fastest dynamics is the rapid establishment of the ϕ profile in the z-direction. As a result, the overall dynamics of the system is determined by a combination of two processes with very different time-scales: the fast process of developing the ϕ profile in the z-direction and the slow suspension flow down the incline. The fast process results in a stationarity of the particle fluxes in the z-direction, allowing us to reconstruct the ϕ and u dependence on z. In the slow process, h and u vary slowly in x, and the dynamics is driven by the conservation laws for the average quantities, e.g. the suspension volume and the number of particles. The free surface curvature terms, i.e. capillary effects, are neglected, making the resulting dynamic equations hyperbolic.

Our model relies on the assumption that the suspension is locally Newtonian. Hence, the particle flux is described via the diffusive flux phenomenology. The main basis for this approach is provided by its successful implementations in previous studies of particle-laden thin-film flows, see Cook (2008) and Murisic *et al.* (2011). The suspension balance approach is yet to be applied to the thin-film setup; however, the similarity in the resulting particle flux for the two approaches was noted in Morris & Boulay (1999). At this point, it is unclear whether the additional complexity resulting from its implementation would yield the corresponding improvement in model predictions compared to the diffusive flux phenomenology. The successful use of the suspension-balance-based models for other setups warrants the comparison between the two approaches for the thin-film flow configuration, but this is beyond the scope of present work.

The particle flux resulting from the diffusive flux approach is empirical. Therefore, different particle flux formulations have appeared in literature. The variety is due to different functional forms of $\mu(\phi)$, and the values of ϕ_m and the flux-related nondimensional coefficients that were used. The mathematical expression for the flux remained largely unchanged between different studies. In the model derivation, we shall maintain generality by postponing the precise definition of the particle flux. Once we define the flux, a general mathematical form will be given, thereby preserving the generality with respect to $\mu(\phi)$ formulation and the relevant parameter values. This will allow us to compare model predictions for several different viscosity/parameter combinations used in literature and examine the sensitivity to these factors.

2.1. *Two-phase model and lubrication equations*

For $0 < z < h(t,x)$, we consider the following system of PDEs for the particle volume fraction ϕ, $0 \le \phi \le \phi_\mathrm{m}$, and the suspension velocity $\mathbf{u}$

$$-\nabla \cdot \left(-P\mathbb{I} + \mu(\phi)(\nabla \mathbf{u} + \nabla \mathbf{u}^\top)\right) = (\rho_p \phi + \rho_\ell (1-\phi))\mathbf{g} \qquad (2.1a)$$

$$\partial_t \phi + \mathbf{u}\cdot\nabla\phi + \nabla\cdot\mathbf{J} = 0, \qquad (2.1b)$$

where the left-hand side of Eq. (2.1a) is divergence of the stress tensor, and the right-hand side takes into account buoyancy with the acceleration of gravity given by $\mathbf{g} = g(\sin\alpha, -\cos\alpha)^\top$. Henceforth, we utilize the notation for partial differentiation: $\partial_t[\cdot] = \frac{\partial}{\partial t}[\cdot]$ etc. As written, Eqs. (2.1) are simply statements of the balance of linear momentum for the suspension (Stokes' equations) and the conservation of particle volume. Here, $\mathbf{J} = (J_x, J_z)^\top$ denotes the particle flux, and it may include shear-induced migration and buoyancy. The importance of shear-induced migration was shown previously in Cook (2008) and Murisic *et al.* (2011). We utilize the diffusive flux approach, but postpone giving the precise definition for $\mathbf{J}$ in order to maintain generality in our model. Similarly, the effective suspension viscosity, $\mu(\phi)$, is kept explicitly in the derivation. Equations (2.1) are accompanied by the incompressibility condition, $\partial_x u + \partial_z w = 0$, and the following boundary conditions: no-slip and impermeability at the solid substrate, $u = w = 0$ at $z = 0$; the zero-stress condition at the free surface, $\left(-P\mathbb{I} + \mu(\phi)(\nabla \mathbf{u} + \nabla \mathbf{u}^\top)\right)\mathbf{n} = 0$ at $z = h$; and the zero-particle-flux conditions at both interfaces, $\mathbf{J}\cdot\mathbf{n} = 0$ at $z = 0$ and $z = h$; here, $\mathbf{n}$ is the outward-poining normal unit vector at the two interfaces. The free surface evolves according to the kinematic condition, $\partial_t h = w - u\partial_x h$ at $z = h$.

Next, we scale (2.1) in the spirit of the lubrication approximation, see e.g. Oron *et al.* (1997), using the following scales

$$[x] = \frac{H}{\varepsilon}, \quad [z] = H, \quad [\phi] = 1, \quad [\mu] = \mu_\ell, \quad [u] = \frac{H^2 \rho_\ell g \sin\alpha}{\mu_\ell} = U$$

$$[w] = \varepsilon[u], \quad [t] = \frac{[x]}{[u]}, \quad [J_z] = \frac{d^2[u]}{[z]^2}, \quad [J_x] = \varepsilon[J_z], \quad [P] = \frac{[u][\mu]}{[z]},$$

where ε is the small lubrication-style parameter to be defined shortly. The motivation for using these particular scales for the particle flux components is provided by the fact that the diffusive flux approach yields $J_x, J_z \propto d^2$, see below; the ε factor in $[J_x]$ is connected to the equilibrium requirement we discuss next.

Assuming that the settling and the suspension velocities are not modified by the hindrance, the typical distance a particle travels in the x-direction as it settles to the solid substrate is given as a product of the relevant time- and velocity-scales

$$\frac{H/\cos\alpha}{U_\mathrm{St}} U = H\left(\frac{d}{H}\right)^{-2} \frac{18\rho_\ell}{\rho_p - \rho_\ell}\tan\alpha \ll \frac{H}{\varepsilon}. \qquad (2.2)$$

Here, we want to derive a continuum model where the particle flux in the z-direction is in equilibrium. The equilibrium assumption is appropriate if the typical distance a particle travels in the x-direction as it settles is asymptotically smaller than the lubrication length scale, $[x]$; hence the inequality in (2.2). Whether it holds is not trivial to answer, revealing some interesting features of these flows. In particular, we focus on the constant suspension volume case. In our experiments the volume is $82.5ml$ and the width of the track is $14cm$; the particles and the suspending liquid are such that $d \approx 360\mu m$ and $(\rho_p - \rho_\ell)/\rho_\ell \approx 1.5$, see §3. The suspension volume may be approximated as a product of the track width, and length-scales H and $[x]$. If $[x] \approx 20cm$, then $H \approx 3mm$ and $\varepsilon \approx 0.015$; the equilibrium condition in (2.2) holds only for extremely small inclination angles. If $[x] \approx 1m$, i.e. the total length of the inclined track in our experiments, then $H \approx 0.6mm$ and $\varepsilon \approx 6 \cdot 10^{-4}$, and the equilibrium assumption is appropriate as long as α is not too close to $90°$. Therefore, the inclination angle is an important parameter in the problem since, for a given setup, there exists a range in α for which the equilibrium assumption is expected to hold. The width of this range increases with the increase in the lubrication length-scale $[x]$. In essence, α dictates how early the equilibrium assumption may be appropriate, while $[x]$ is the typical displacement of the suspension front in the x-direction measured from the top of the incline and relevant to the flow in equilibrium.

In §3, we shall discuss an early-time transient observed in our experiments where the suspension is well-mixed, the flow is unsteady and the equilibrium assumption is not applicable. The experiments will confirm that the duration of the transient stage is proportional to α. One may estimate the distance traveled by the suspension front during this transient stage by using (2.2) and the above approximation for the total suspension volume: e.g. for $\alpha = 10°$ it is $\approx 25cm$ and for $\alpha = 25°$ it is $\approx 30cm$, both $< 1m$ and in agreement with our experimental observations, see §3. At long times, the films in finite volume flows become very thin, $(d/H) \to 1$, and the continuum hypothesis breaks down. For $(d/H) \to 0$, the transport of the particles is purely convective, the settling time-scale goes to infinity, and the suspension behaves like a colloid. In order to enforce the continuum assumption we require that $(d/H)^2 \ll 1$. In our flows, $(d/H)^2 \sim \mathcal{O}(10^{-2})$ at the end of the early-time transient. We also note that (2.2) effectively estimates buoyancy strength since it considers a ratio of velocity scales relevant to shearing and settling, similar to Morris & Brady (1998). Namely, the strength of buoyancy relative to the shearing force is $(d/H)^2(\rho_p - \rho_\ell)/(18\rho_\ell \tan\alpha)$, typically an $\mathcal{O}(10^{-2})$ quantity when the equilibrium assumption holds.

The conditions for continuum and equilibrium are combined into a single requirement

$$\varepsilon \ll \left(\frac{d}{H}\right)^2 \ll 1. \tag{2.3}$$

The equilibrium part is an approximate version of (2.2): to simplify the formal asymptotics that we present next, the pre-factor $18\rho_\ell \tan\alpha/(\rho_p - \rho_\ell)$ is neglected. We note here that the usefulness of (2.3) becomes questionable when α is large. The equilibrium condition may also be obtained by requiring that the z-component of the particle flux $\mathbf{J}$ dominates in the scaled version of (2.1b). This leads to equilibrium in the z-direction at the leading order. As the evolution proceeds the equilibrium assumption is expected to be increasingly appropriate. At late times when the film is very thin, the continuum condition is eventually violated; this will limit us in describing the long time dynamics. Mathematically, a way to satisfy (2.3) is to set $(d/H)^2 = \varepsilon^\beta$ where $0 < \beta < 1$. Applying the scales to (2.1b), while keeping in mind the definition of β, gives

$$\partial_t \phi + u\partial_x \phi + w\partial_z \phi = -\varepsilon^{\beta+1}\partial_x J_x - \varepsilon^{\beta-1}\partial_z J_z. \tag{2.4}$$

Henceforth, all dependent and independent variables are listed in their nondimensional form unless otherwise noted. We proceed by defining the asymptotic expansions of the solution: $\phi(t,x,z) = \phi^0(t,x,z) + o(1)$, $u(t,x,z) = u^0(t,x,z) + o(1)$, $w(t,x,z) = w^0(t,x,z) + o(1)$, $h(t,x) = h^0(t,x) + o(1)$, $J_x(t,x,z) = J_x^0(t,x,z) + o(1)$, and $J_z(t,x,z) = J_z^0(t,x,z) + o(1)$. Here, $\phi^0, u^0, w^0, h^0, J_x^0, J_z^0 \sim \mathcal{O}(1)$. After using these expansions in (2.4), the leading order term is $\mathcal{O}(\varepsilon^{\beta-1})$, describing the effect of the most dominant particle flux, J_z^0. Integrating the resulting leading order equation with respect to z and employing either of the zero-flux boundary conditions yields

$$J_z^0(t,x,z) = 0. \tag{2.5}$$

This is complemented by the zero-flux boundary conditions, $J_z^0|_{z=0}, J_z^0|_{z=h^0} = 0$. By employing a similar approach on (2.1a) we obtain

$$\partial_z\big(\mu(\phi^0)\partial_z u^0\big) = -(1 + \frac{\rho_p - \rho_\ell}{\rho_\ell}\phi^0), \tag{2.6}$$

accompanied by the no-slip and zero-stress boundary conditions, $u^0 = 0$ at $z = 0$, and $\mu(\phi^0)\partial_z u^0 = 0$ at $z = h^0$ respectively. We note that Cook (2008) used an alternate but equivalent approach to deriving (2.5): a steady-state in the z-direction was assumed from the beginning so that the z-component of the particle flux could be set to zero; (2.5) was then obtained by using the zero-flux boundary conditions.

2.2. *Particle transport model*

Equations (2.5) and (2.6) are similar to the ones previously derived in Cook (2008) and Murisic *et al.* (2011): they constitute the equilibrium model for the particle settling. This model has a one-parameter family of solutions that may be parameterized by the integrated volume fraction of particles

$$n(t,x) = \int_0^{h^0} \phi^0(t,x,z)\,\mathrm{d}z. \tag{2.7}$$

Once n is fixed and the form of flux J_z^0 is known, the z-dependence of ϕ^0 and u^0 may be determined uniquely from (2.5) and (2.6), and the accompanying boundary conditions. To indicate that the dependence of the solution on z at the leading order is only parametrical through n, we write $\phi^0 = \phi^0(t,x;z)$ and $u^0 = u^0(t,x;z)$. We note that the initial value $n(0,x)$ may be obtained using the initial data, but the time-dependence of n is still unknown at this point. In order to determine it, we consider higher order terms in (2.4) including the correction for the z-direction particle flux

$$\partial_t \phi^0 + u^0\partial_x \phi^0 + w^0\partial_z \phi^0 = \varepsilon^{\beta-1}\partial_z\left(J_z - J_z^0\right). \tag{2.8}$$

This may be integrated in the z-direction from $z = 0$ to $z = h^0$ to obtain a closed form and cast the dynamic and equilibrium models into a single framework. The flux correction term drops out due to the zero-flux boundary conditions. Using the kinematic condition, $\partial_t h^0 = w^0 - u^0\partial_x h^0$ at $z = h^0$, and $\partial_t \int_0^{h^0} \phi^0 dz = \phi^0\partial_t h^0|_{z=h^0} + \int_0^{h^0} \partial_t\phi^0 dz$ gives

$$\partial_t \int_0^{h^0} \phi^0 dz = \phi^0(w^0 - u^0\partial_x h^0)|_{z=h^0} - \int_0^{h^0} u^0\partial_x\phi^0 dz - \int_0^{h^0} w^0\partial_z\phi^0 dz.$$

After using the chain rule, the property $\partial_x \int_0^{h^0} \phi^0 u^0 dz = \phi^0 u^0 \partial_x h^0|_{z=h^0} + \int_0^{h^0} \partial_x \left(\phi^0 u^0\right) dz$ and integration by parts, and applying the impermeability and incompressibility conditions, $w^0|_{z=0} = 0$ and $\partial_x u^0 + \partial_z w^0 = 0$ respectively, we get

$$\partial_t \int_0^{h^0} \phi^0 dz + \partial_x \int_0^{h^0} \phi^0 u^0 dz = 0.$$

Finally, recalling the definition of n gives an advection equation for the particle number, i.e. a conservation law for the particles

$$\partial_t n + \partial_x \int_0^{h^0} \phi^0(t,x;z) u^0(t,x;z)\,\mathrm{d}z = 0. \tag{2.9a}$$

A similar standard lubrication theory argument gives the conservation law for the suspension volume

$$\partial_t h^0 + \partial_x \int_0^{h^0} u^0(t,x;z)\,\mathrm{d}z = 0. \tag{2.9b}$$

The conservation laws similar to (2.9) were given in Murisic *et al.* (2011) without formal derivation. That these laws are hyperbolic is shown below. Equations (2.5), (2.6) and (2.9) together with the boundary conditions, $u^0 = 0$ at $z = 0$, $J_z^0|_{z=0}, J_z^0|_{z=h^0} = 0$, and $\mu(\phi^0)\partial_z u^0 = 0$ at $z = h^0$, provide the full theoretical framework.

Next, we give the functional form for the particle flux $\mathbf{J}$. We follow Leighton & Acrivos (1987*b*), Phillips *et al.* (1992), Cook (2008) and Murisic *et al.* (2011), and consider a general particle flux expression (dimensional form) based on the diffusive flux phenomenology

$$\mathbf{J} = -\frac{d^2}{4}\left[K_c \phi \begin{pmatrix} \partial_x(\dot\gamma\phi) \\ \partial_z(\dot\gamma\phi)\end{pmatrix} + \frac{K_v \phi^2 \dot\gamma}{\mu(\phi)}\frac{d\mu(\phi)}{d\phi}\begin{pmatrix}\partial_x\phi \\ \partial_z\phi\end{pmatrix}\right] + \frac{d^2(\rho_p - \rho_\ell)\Phi(\phi)}{18\mu(\phi)}\phi\mathbf{g}.$$

Shear-induced migration is included via the terms in the first brackets and the hindered settling of particles due to gravity via the remaining term; the effective suspension viscosity $\mu(\phi)$ and the hindrance function $\Phi(\phi)$ are kept explicitly. Empirical constants K_c and K_v multiply the contributions to the shear-induced particle flux due to gradients in the particle volume fraction and the effective suspension viscosity respectively. Their values are estimated by choosing an appropriate expression for $\mu(\phi)$ and comparing the model predictions and experiments, see e.g. Leighton & Acrivos (1987*b*). We will later consider different combinations of K_c, K_v values and $\mu(\phi)$ expressions, and examine their influence on the model predictions. The hindrance to settling due to the wall-effect, see Murisic *et al.* (2011), is neglected here. The shear rate is given as usual, $\dot\gamma = \frac{1}{4}\|\nabla\mathbf{u} + \nabla\mathbf{u}^\top\| \approx |\partial_z u^0|$. We also neglect the contribution to the particle flux due to Brownian motion since the relevant Péclet number is large, as shown above. After using previously defined scales and asymptotic expansions, we get

$$J_z^0 = -\frac{K_c}{4}\phi^0\partial_z\left(\phi^0\partial_z u^0\right) - \frac{K_v}{4}\frac{(\phi^0)^2\partial_z u^0 \partial_z\phi^0}{\mu(\phi^0)}\frac{d\mu(\phi^0)}{d\phi^0} - \frac{(\rho_p - \rho_\ell)\,\Phi(\phi^0)\phi^0\cot\alpha}{18\rho_\ell\mu(\phi^0)}.$$

This is substituted into Eq. (2.5), rewriting the equilibrium model in terms of the stress $\sigma^0 = \mu(\phi^0)\partial_z u^0$

$$\phi^0\partial_z\sigma^0 + \left(1 + \frac{\phi^0}{\mu(\phi^0)}\frac{d\mu(\phi^0)}{d\phi^0}\frac{K_v - K_c}{K_c}\right)\sigma^0\partial_z\phi^0 + \frac{2\,(\rho_p - \rho_\ell)\,\Phi(\phi^0)\cot\alpha}{9\rho_\ell K_c} = 0 \tag{2.10a}$$

$$\partial_z\sigma^0 = -(1 + \frac{\rho_p - \rho_\ell}{\rho_\ell}\phi^0). \tag{2.10b}$$

Here, the magnitudes of both shear-induced migration parameters are relevant. In contrast, in the case of neutrally buoyant particles, only their ratio, K_v/K_c, plays a role. This feature of our model may be useful for determining the appropriate magnitudes of K_c and K_v via comparison with experiments, focusing on the early-time transient regime, see §3. Equations (2.9) may be simplified by removing the explicit dependence on h from (2.10). This is achieved by a change of variables from z to $s = z/h^0$. Henceforth, we omit the "0" superscripts for simplicity. Equations (2.9) are then rewritten using $\phi(t,x;z) = \phi(t,x;h(t,x)s) = \tilde{\phi}(t,x;s)$, $u(t,x;z) = u(t,x;h(t,x)s) = h(t,x)^2\tilde{u}(t,x;s)$, and $\tilde{\sigma}(t,x;s) = \sigma(t,x;h(t,x)s)/h(t,x) = \mu(\tilde{\phi}(t,x;s))\tilde{u}'(t,x;s)$. The prime from here on denotes the differentiation with respect to s. The result is

$$\partial_t h + \partial_x F(h,n) = 0 \tag{2.11a}$$

$$\partial_t n + \partial_x G(h,n) = 0, \tag{2.11b}$$

where the suspension and particle fluxes, F and G, are written in terms of $\tilde{\phi}$ and $\tilde{u}$

$$F(h,n) = \int_0^h u(t,x;z)\mathrm{d}z = h^3 \int_0^1 \tilde{u}(t,x;s)\,\mathrm{d}s = h^3 f(\phi_0) \tag{2.11c}$$

$$G(h,n) = \int_0^h \phi(t,x;z)u(t,x;z)\mathrm{d}z = h^3 \int_0^1 \tilde{\phi}(t,x;s)\tilde{u}(t,x;s)\,\mathrm{d}s = h^3 g(\phi_0), \tag{2.11d}$$

and the vertically-averaged particle volume fraction is

$$\phi_0(t,x) = \int_0^1 \tilde{\phi}(t,x;s)\,\mathrm{d}s = \frac{n(t,x)}{h(t,x)} \in [0,\phi_{\mathrm{m}}]. \tag{2.11e}$$

The hindrance function we use here is $\Phi(\tilde{\phi}) = (1-\tilde{\phi})$, appropriate in the presence of shear, see Schaflinger *et al.* (1990). The equilibrium equations are then rewritten as

$$\left(1 + \frac{\tilde{\phi}}{\mu(\tilde{\phi})}\frac{d\mu(\tilde{\phi})}{d\tilde{\phi}}\frac{K_v - K_c}{K_c}\right)\tilde{\sigma}\tilde{\phi}' + B - (B+1)\tilde{\phi} - \frac{\rho_p - \rho_\ell}{\rho_\ell}\tilde{\phi}^2 = 0, \tag{2.11f}$$

$$\tilde{\sigma}' = -(1 + \frac{\rho_p - \rho_\ell}{\rho_\ell}\tilde{\phi}), \tag{2.11g}$$

for $0 \le s \le 1$, with the boundary condition $\tilde{\sigma}(1) = 0$. Here, $B = 2(\rho_p - \rho_\ell)\cot\alpha/(9\rho_\ell K_c)$ is a nondimensional buoyancy parameter measuring the strength of settling due to gravity in the z-direction relative to the strength of shear-induced migration. We note that $B \sim \mathcal{O}(1)$ for relevant α values; the coefficient $(\rho_p - \rho_\ell)/\rho_\ell$ and the combined terms multiplying $\tilde{\sigma}\tilde{\phi}'$ are also $\sim \mathcal{O}(1)$. The equilibrium model, (2.11f) and g), is solved for the intermediate variables $\tilde{\sigma}$ and $\tilde{\phi}$; $\tilde{u}$ is recovered from $\tilde{\sigma} = \mu(\tilde{\phi})\tilde{u}'$ using the no-slip boundary condition at $s = 0$. These profiles are then supplied to the transport equations (2.11a-e) to close the system: the suspension and the particle fluxes are determined by the functions f and g of a single real argument, that are found by solving (2.11f) and g) for $s \in [0,1]$ and a given value of ϕ_0. We note that the cubic dependence of the fluxes F and G on h, reminiscent of the factors appearing in the thin film equation, e.g. see Oron *et al.* (1997), results from the exact scaling invariance of the leading order ODEs.

For a given value of ϕ_0, the physically meaningful non-negative solution to the system (2.11f) and g) is unique. Within this one-parameter family, two distinct types of solutions exist. The first type occurs for smaller ϕ_0 values and it is characterized by monotonically decreasing $\tilde{\phi}$ profiles. In particular, with $0 < \tilde{T} = T/h < 1$, the resulting $\tilde{\phi}(s)$ is strictly decreasing for $0 \le s \le \tilde{T}$, leading to $\tilde{\phi}(\tilde{T}) = 0$. Since $J_z \equiv 0$ for $\tilde{\phi} = 0$ and any $\tilde{\sigma}$ and $\tilde{\phi}'$, the solution is then continued with $\tilde{\phi}(s) = 0$ for $\tilde{T} < s < 1$ to obtain physically meaningful non-negative profile; once ϕ_0 is given, this solution is unique. The second type of solutions occurs for larger values of ϕ_0 and it is characterized by strictly increasing $\tilde{\phi}(s)$ profiles, where $\tilde{\phi}(s) \to \phi_{\mathrm{m}}$ as $s \to 1$. Here, the focus is solely on the first type of solutions, since it corresponds to the settled regime, expected for small values of α and ϕ_0. The second type corresponds to the ridged regime; see Figs. 3 and 5 below for more detail regarding the two solution types. The critical volume fraction, $\tilde{\phi}_{crit}$, separating the two extreme regimes, is determined by the constant-concentration solution, i.e. setting $\tilde{\phi}' = 0$ in (2.11f), and solving for the average particle volume fraction

$$\tilde{\phi}_{crit} = \min\left\{\phi_{\mathrm{m}}, \frac{-\rho_\ell(B+1)}{2(\rho_p-\rho_\ell)} + \sqrt{\left(\frac{\rho_\ell(B+1)}{2(\rho_p-\rho_\ell)}\right)^2 + \frac{\rho_\ell B}{\rho_p-\rho_\ell}}\right\}. \tag{2.12}$$

This expression defines the transient well-mixed state. A different type of well-mixed transient, due to initial data, will be discussed below.

2.3. *Effective suspension viscosity and particle flux*

Next, we discuss several choices for the effective suspension viscosity $\mu(\tilde{\phi})$ and the values of the parameters ϕ_m, K_c and K_v that result in different particle fluxes $\mathbf{J}$. Our goal is to use different but realistic combinations in order to examine the sensitivity of model predictions on this choice. The five different combinations we consider are as follows.

- 'Einstein': based on

$$\mu(\tilde{\phi}) = 1 + \frac{5}{2}\tilde{\phi},$$

derived analytically in Einstein (1906, 1911) for dilute suspensions, i.e. $\phi_0, \tilde{\phi} \to 0$. We pair this $\mu(\tilde{\phi})$ with $K_c = 0.41$ and $K_v = 0.62$ from Murisic *et al.* (2011). This combination is employed to investigate the impact of a very coarse suspension viscosity approximation on the model predictions.

- 'Acrivos & Leighton': uses the empirical Eilers formula from Eilers (1941) and Ferrini *et al.* (1979)

$$\mu(\tilde{\phi}) = \left(1 + \frac{1}{2}\frac{\eta\tilde{\phi}}{1 - \frac{\tilde{\phi}}{\phi_m}}\right)^2.$$

In Leighton & Acrivos (1987*b*), it was utilized for particle-laden flows in a Couette device with $\eta = 3.0$, $\phi_m = 0.58$, $K_c = 0.41$ and $K_v = 0.61$.

- 'Phillips et al.': relies on a simplified version of Eilers formula, known as the Krieger-Dougherty relation, see Krieger & Dougherty (1959)

$$\mu(\tilde{\phi}) = \left(1 - \frac{\tilde{\phi}}{\phi_m}\right)^{-\psi}.$$

This empirical relation was used in Phillips *et al.* (1992) to model particle-laden flows in a Couette device with $\phi_m = 0.68$, $\psi = 1.82$, $K_c = 0.41$ and $K_v = 0.62$.

- 'Merhi et al.': also utilizes the Krieger-Dougherty relation. In Merhi *et al.* (2005) it was employed to study suspensions in a Couette flow with $\phi_m = 0.68$, $\psi = 1.82$, $K_c = 0.105$ and $K_v = 0.525$.

- 'Murisic et al.': the main combination here. It is based on the so-called Maron-Pierce relation – the Krieger-Dougherty relation with $\psi = 2$, see Maron & Pierce (1956). It was used with $\phi_m = 0.61$, $K_c = 0.41$ and $K_v = 0.62$ in Murisic *et al.* (2011) to successfully

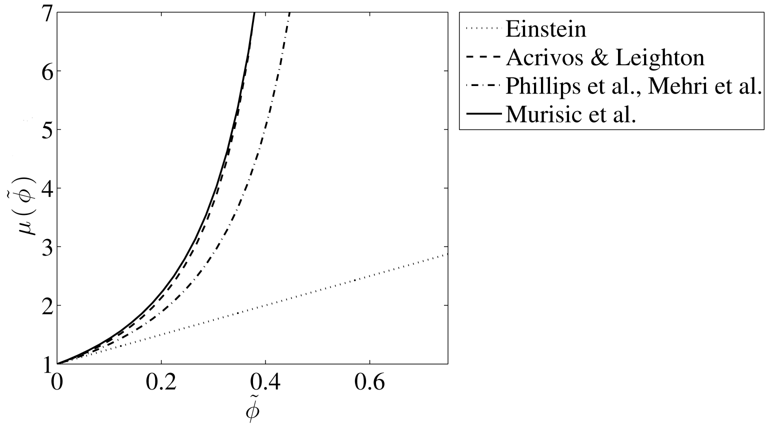

FIGURE 2. Comparison of different suspension viscosity models used in literature. Our main focus in this work is on the Maron-Pierce relation from Murisic *et al.* (2011).

model particle-laden thin-film flows on an incline. After the comparison, we shall focus solely on this combination.

First, we compare the $\mu(\tilde{\phi})$ profiles for the Einstein expression, the Eilers formulation as in Leighton & Acrivos (1987*b*), the Krieger-Dougherty relation as in Phillips *et al.* (1992) and Merhi *et al.* (2005), and the Maron-Pierce relation as in Murisic *et al.* (2011). The results are given in Fig. 2. The Einstein expression, as expected, is useful only for very small particle volume fractions. Namely, it already deviates from other viscosity models by a factor of 2 for concentrations as small as $\tilde{\phi} = 0.1$. The three remaining relations give similar profiles. The agreement between the Eilers and Maron-Pierce relations is somewhat surprising. While the two relations clearly differ mathematically, the parameter values used give very similar viscosity profiles in the considered $\tilde{\phi}$ range.

Next, we substitute the listed combinations into the governing system, Eqs. (2.11), in order to study their influence on the model predictions. The solutions are obtained numerically using a shooting method, see Murisic *et al.* (2011). The results of this comparison are shown in Figs. 3 and 4. Figures 3a) and b) focus on $\tilde{\phi}(s)$ and $\tilde{u}(s)$ profiles respectively for $\phi_0 = 0.2$ and $\alpha = 20°$. All combinations give qualitatively similar profiles. With the exception of the 'Einstein' combination, which is not expected to be very appropriate at $\phi_0 = 0.2$, all other combinations are also quantitatively close to one another. The crude suspension viscosity approximation in the 'Einstein' combination has only a mild effect on the $\tilde{\phi}(s)$ profile; unsurprisingly, it has a rather substantial effect on the $\tilde{u}(s)$ profile. Figures 3a) and b) indicate that once, e.g. the viscosity model is chosen, K_c and K_v values may be tuned to obtain desired $\tilde{\phi}(s)$ and $\tilde{u}(s)$ profiles. Such an approach was previously used e.g. in Leighton & Acrivos (1987*b*). We note that the profiles for 'Acrivos & Leighton' and 'Murisic et al.' almost coincide, as one may have anticipated based on the results from Fig. 2. In Figs. 3c) and d) we compare the resulting suspension and particle fluxes for $\alpha = 20°$ and different values of ϕ_0. Clearly, the 'Einstein' combination ceases to be appropriate for all but very small ϕ_0 values. The other combinations give qualitatively similar behavior, with 'Acrivos & Leighton' and 'Murisic et al.' again very close to one another. A more detailed discussion of $f(\phi_0)$ and $g(\phi_0)$ profiles is given below. Finally, in Fig. 4, we compare the model predictions for clear liquid film and particle front positions in the settled regime for $\phi_0 = 0.2$ and $\alpha = 20°$. The initial data used for all simulations corresponds to a well-mixed suspension in the reservoir at $t = 0$. The

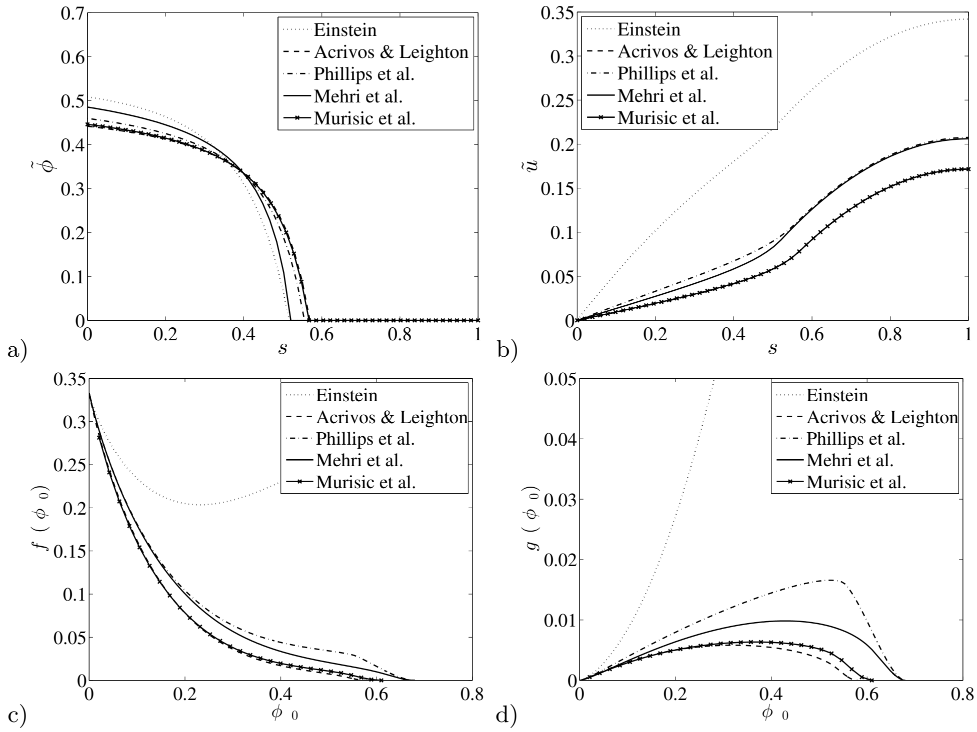

FIGURE 3. Particle volume fraction in a) and suspension velocity profiles in b) at $\phi_0 = 0.2$ and $\alpha = 20°$ for different viscosity/parameters combinations. Suspension and particle fluxes are compared in c) and d) respectively for $\alpha = 20°$. Our model will rely on the 'Murisic et al.' combination in subsequent analysis.

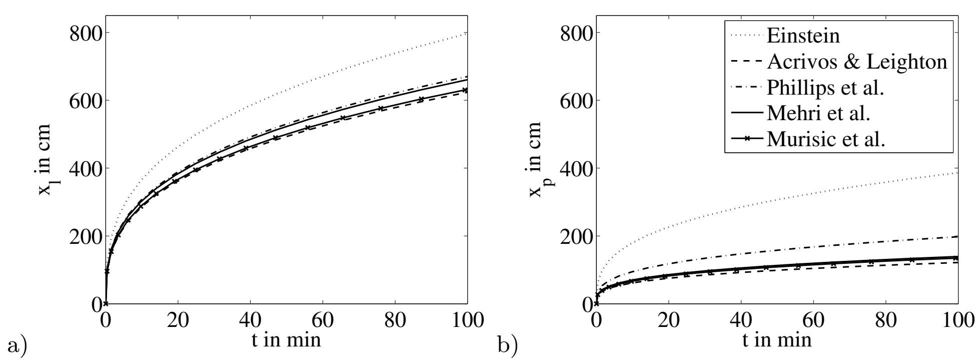

FIGURE 4. The evolution of the clear liquid and particle front positions x_ℓ and x_p for different viscosity/parameters combinations: $\phi_0 = 0.2$ and $\alpha = 20°$; the legend in b) applies to a) too.

'Einstein' combination deviates from the others significantly. This is not surprising due to the results in Figs. 2 and 3: it underestimates μ and hence overestimates $\tilde{u}$ and the fluxes. All other combinations give results that are close to one another. Of the three, the 'Phillips et al.' combination predicts the fastest fronts. 'Acrivos & Leighton' and 'Murisic et al.' give essentially identical predictions. For long times, all combinations yield front positions that exhibit the Huppert-like $t^{1/3}$ behavior.

Based on Figs. 3 and 4, any combination may be applicable excluding 'Einstein', which is clearly not adequate here due to its poor prediction of suspension velocity. We choose

'Murisic et al.' owing to its success when used for particle-laden thin-film flows. In Murisic *et al.* (2011), an equilibrium model similar to (2.11f) and g) gave predictions that were in excellent agreement with the experimental data for a wide range of ϕ_0 and α values. We note that this particular combination may not be applicable for some other physical setups or flow geometries – tuning of parameters, e.g. K_c and K_v may be required, as suggested by Merhi *et al.* (2005). Henceforth, we only consider this combination and discuss various predictions of our model based on it. The full governing system consists of (2.11a-e) together with the equilibrium equations (2.11f) and g), which may be rewritten using the 'Murisic et al.' combination as

$$\left(1+\frac{2\,(K_v-K_c)}{K_c}\frac{\tilde{\phi}}{\phi_{\mathrm{m}}-\tilde{\phi}}\right)\tilde{\sigma}\tilde{\phi}'+B-(B+1)\tilde{\phi}-\frac{\rho_p-\rho_\ell}{\rho_\ell}\tilde{\phi}^2=0, \tag{2.13a}$$

$$\tilde{\sigma}'=-(1+\frac{\rho_p-\rho_\ell}{\rho_\ell}\tilde{\phi}), \tag{2.13b}$$

for $0\le s\le 1$, with the boundary condition $\tilde{\sigma}(1)=0$.

We proceed by examining the $\tilde{\phi}(s)$ and $\tilde{u}(s)$ profiles in more detail. Figures 5a) and b) show two families of solutions for $\tilde{\phi}$ depending on the ϕ_0 and α value, including the well-mixed state occurring for $\tilde{\phi}_{crit}$ in a); corresponding suspension velocity $\tilde{u}(s)$ profiles are given in c) and d). For small values of ϕ_0, the $\tilde{\phi}(s)$ profiles are monotonically decreasing while $\tilde{u}(s)$ profiles are increasing in s. This corresponds to the settled regime with the velocity $\tilde{u}$ largest in the particle-free layer $\tilde{T}<s\le 1$. Hence, the equilibrium theory essentially predicts the faster flow of the clear liquid front compared to the particles for small values of ϕ_0. To see this more clearly, note that the suspension and particle fluxes in the transport equations (2.11a) and b) are computed directly from the equilibrium profiles $\tilde{\phi}(s)$ and $\tilde{u}(s)$. As a result, when $\phi_0<\tilde{\phi}_{crit}$, the faster clear liquid layer leaves the particulate bed behind, yielding two distinct fronts. For $\phi_0>\tilde{\phi}_{crit}$, the $\tilde{\phi}(s)$ profiles are monotonically increasing with s, i.e. the particles gather at the free surface; the corresponding $\tilde{u}(s)$ profiles, while small in magnitude, are still monotonically increasing. Since the fluxes f and g are calculated directly from $\tilde{\phi}(s)$ and $\tilde{u}(s)$ profiles, $\phi_0>\tilde{\phi}_{crit}$ results in the ridged regime: the particles in this case flow faster than the liquid leading to their accumulation at the suspension front. We proceed by studying the dilute approximation of the governing system, relevant for the settled regime.

2.4. *Dilute approximation*

For small particle concentrations, we may compute the fluxes analytically. Assuming $\phi_0,\tilde{\phi}(s)\ll\phi_{\mathrm{m}}$, we linearize (2.13) with respect to $\tilde{\phi}$ and to the leading order obtain

$$\tilde{\sigma}\tilde{\phi}'=-B \qquad 0\le s\le\tilde{T} \tag{2.14}$$

$$\tilde{\sigma}'=-1 \qquad 0\le s\le 1, \tag{2.15}$$

with $\tilde{\sigma}(1)=0$. To the leading order in $\tilde{\phi}$, the solution to this system is

$$\tilde{\sigma}(s)=1-s \tag{2.16}$$

$$\tilde{\phi}(s)=\begin{cases}B(\tilde{T}-s) & 0<s\le\tilde{T}\\ 0 & \tilde{T}<s\le 1,\end{cases} \tag{2.17}$$

resulting in the average particle volume fraction

$$\phi_0=\int_0^1\tilde{\phi}(s)\,\mathrm{d}s=\frac{B\tilde{T}^2}{2}. \tag{2.18}$$

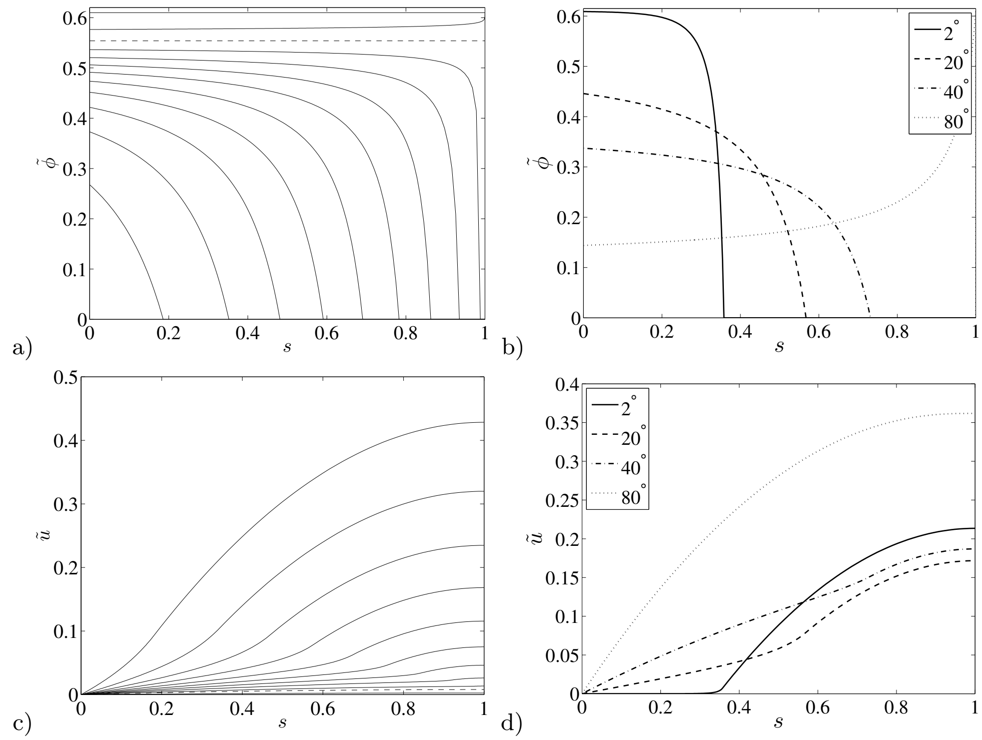

FIGURE 5. Particle volume fraction profiles in a) and b), and the corresponding suspension velocity profiles in c) and d) for different values of α and ϕ_0. In a) and c), $\alpha = 20^\circ$ is fixed and ϕ_0 is increased from 0 to ϕ_{m} via $\tilde{\phi}_{crit} = 0.554$ (dashed line). The $\tilde{\phi}$ magnitudes in a) increase, while $\tilde{u}$ magnitudes in c) decrease with ϕ_0. In b) and d), $\phi_0 = 0.2$ is fixed and α is varied.

By using $\tilde{\sigma} = \mu(\tilde{\phi})\tilde{u}' \approx \mu(0)\tilde{u}'$, the velocity $\tilde{u}(s)$ to the leading order is

$$\tilde{u}(s) = \int_0^s \frac{\tilde{\sigma}(r)}{\mu(\tilde{\phi}(r))}\,\mathrm{d}r = \int_0^s \frac{(1-r)}{\mu(0)}\left(1 + \mathcal{O}(\tilde{\phi})\right)\,\mathrm{d}r = \left(s - \frac{s^2}{2}\right) + \mathcal{O}(\phi_0).$$

Employing (2.18) yields the particle flux to the leading order

$$\begin{aligned} g(\phi_0) &= \int_0^1 \tilde{\phi}(s)\tilde{u}(s)\,\mathrm{d}s = \int_0^{\tilde{T}} B(\tilde{T}-s)\left(s - \frac{s^2}{2}\right)\,\mathrm{d}s \\ &= B\left(\frac{\tilde{T}^3}{6} - \frac{\tilde{T}^4}{24}\right) = \sqrt{\frac{2}{9B}}\phi_0^{3/2} + \mathcal{O}(\phi_0^2). \end{aligned} \tag{2.19}$$

Also, the suspension volume flux to the leading order is

$$f(\phi_0) = \int_0^1 \tilde{u}(s)\,\mathrm{d}s = \frac{1}{3}. \tag{2.20}$$

Finally, to the leading order, the hyperbolic transport laws in the dilute limit are

$$\partial_t h + \partial_x\left(\frac{h^3}{3}\right) = 0, \tag{2.21a}$$

$$\partial_t n + \partial_x\left(\sqrt{\frac{2}{9B}}(nh)^{3/2}\right) = 0. \tag{2.21b}$$

The regime where two distinct fronts occur, with the clear liquid front being faster, has already been predicted by our equilibrium model for $\phi_0 < \tilde{\phi}_{crit}$, see Fig. 5. The two fronts scenario with a faster liquid front is inevitable in the dilute limit since the relevant fluxes are computed directly from the equilibrium profiles $\tilde{\phi}(s)$ and $\tilde{u}(s)$. The average particle and volume velocities are effectively encoded into these flux expressions. As long as $\tilde{u}(s)$ is monotonically increasing and $\tilde{\phi}(s)$ decreasing, the particles on average move slower than the liquid and a clear liquid front traveling ahead of a particles front emerges from the conservation laws – this is an intrinsic property of the settled regime. This could also be seen by comparing the fluxes: the liquid front will be faster than the particle one provided $f(\phi_0) > g(\phi_0)/\phi_0$, a condition satisfied in the dilute limit.

We proceed by solving (2.21) exactly for the fixed suspension volume case, with the initial data $h(0,x) = 1$ for $0 \le x \le 1$, $h(0,x) = 0$ otherwise, $n(0,x) = f_0 h(0,x)$, and some given value of $f_0 \ll 1$. Since ϕ_0 is small in the dilute limit, we solve (2.21a) for h independently to get

$$h(t,x) = \begin{cases} 1 & t \le x \le x_\ell(t) \\ \sqrt{x/t} & 0 < x < \min\big(t, x_\ell(t)\big) \\ 0 & \text{else,} \end{cases} \tag{2.22}$$

for $t \ge 0$, where the liquid front position is

$$x_\ell(t) = \begin{cases} 1 + t/3 & 0 \le t \le 3/2 \\ \left(\frac{9t}{4}\right)^{1/3} & 3/2 < t. \end{cases}$$

This is the well-known solution from Huppert (1982). Next, we use it to find the solution for n. First note that for early times, the solution for n also consists of a rarefaction fan for $0 < x < t$, connected to a constant with value f_0 in $t \le x \le 1 + (f_0^{1/2} t)/\sqrt{2B}$. For larger values of x, the integrated particle volume fraction n vanishes. The evolution equation for n may be written as

$$\partial_t n + \frac{2}{3\sqrt{2B}} \partial_x \big(h(t,x) n(t,x)\big)^{3/2} = 0. \tag{2.23}$$

Note that by the assumption of dilute regime, we always have $x_p < x_\ell$. Clearly, the problem amounts to determining the shape of the rarefaction fan for n. To resolve it, we assume that $n(t,x) = N(x/t)$ is a rarefaction fan starting at zero, i.e. $x/t > 0$. Substituting this ansatz into (2.23) gives the following ODE for N

$$-2\left(\frac{x}{t}\right)^{5/4} N'(x/t) + \sqrt{\frac{N(x/t)}{2B}}\left[N(x/t) + 2\frac{x}{t} N'(x/t)\right] = 0, \tag{2.24}$$

solved by

$$N(x/t) = \frac{C}{\sqrt{\frac{x}{t}}}\left(\sqrt{2B\frac{x}{t}} - 2\sqrt{C^2 + C\sqrt{2B\frac{x}{t}}} + 2C\right),$$

where C is an undetermined constant of integration. This solution satisfies $N(x/t) \to 0$ as $x/t \to 0$. For our purposes we may fix C by requiring that the continuity is obeyed, i.e. $n(t,t) = N(1) = f_0$, resulting in $C = f_0/(\sqrt{2B} - 2\sqrt{f_0})$. Hence, the value for C in general depends on the initial data. Our solution is given by

$$n(t,x) = \begin{cases} f_0 & t \le x \le x_p(t) \\ N(x/t) & 0 < x < \min\big(t, x_p(t)\big) \\ 0 & \text{else,} \end{cases} \tag{2.25}$$

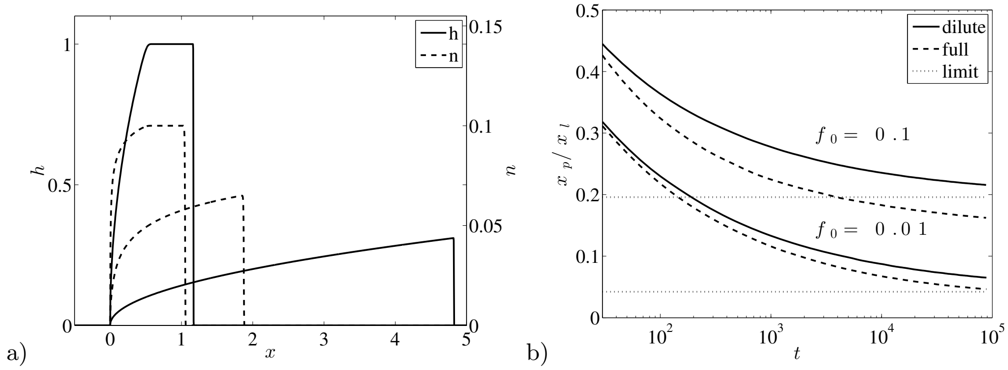

FIGURE 6. Exact solution in the dilute limit in a) shows the clear liquid and particle fronts at $t = 0.5$ and $t = 50$ (direction of flow is left to right); here, $B = 2.307$ ($\alpha = 20°$) and $f_0 = 0.1$. Exact solution for dilute approximation vs. numerical solution of the full model in b): $x_p(t)/x_\ell(t)$ for $B = 2.307$ and different values of f_0; dotted lines are the corresponding $t \to \infty$ limits.

and the particle front position is $x_p(t) = \min(1+2t\sqrt{f_0}/(3\sqrt{2B}), \bar{x}_p(t))$, where $\bar{x}_p$ satisfies

$$\int_0^{\bar{x}_p} N(x/t)\,\mathrm{d}x = f_0. \tag{2.26}$$

Using $\bar{x}_p/t \to 0$ as $t \to \infty$ and $N(x/t) = \frac{1}{2}B\sqrt{x/t} + \mathcal{O}(x/t)$ we get $\bar{x}_p(t) = (9f_0^2 t/B^2)^{1/3}$. Therefore,

$$\lim_{t\to\infty} \frac{x_p(t)}{x_\ell(t)} = \left(\frac{4f_0^2}{B^2}\right)^{1/3}.$$

We note that the value of this limit is independent of the choice for C. Here, $N(x/t)$ is the generic candidate for describing the long-time evolution of the particle distribution. Namely, while $N(x/t)$ is determined by the mechanisms responsible for fixing the value of C at early times, its expansion as $x/t \to 0$, i.e. as $t \to \infty$, is independent of C. Figure 6a) shows the exact solution of (2.21), indicating that the clear liquid front is indeed faster than the particle one in the dilute limit.

Another type of transient is uncovered here – due to the shape of the initial data. This transient is different from the experimentally observed transient that is connected to the equilibrium assumption in our model, see §3. The presence of the initial data transient conceals the $x_p \sim t^{1/3}$ behavior for early times. To examine this further, we expand N to next order in x/t and derive the correction: $\bar{x}_p \sim (9f_0^2 t/B^2)^{1/3} + (3/2 - 3\sqrt{f_0/(2B)}) + \mathcal{O}(t^{-1/3})$. The duration of the transient is therefore $t \sim f_0^{-2}$, a very long time for $f_0 \ll 1$ relevant here. Hence the long-time comparison between the exact solution in the dilute limit and the numerical solution of the full model in Fig. 6b): it takes a while for the exact solution to reach the calculated $t \to \infty$ limit when $f_0 = 10^{-2}$. This transient is likely to affect the model predictions even outside of the dilute limit. Both transients – due to the initial data and the early-time unsteady nature of the flow in the experiments – will affect the comparison between model predictions and experiments discussed in §4. Next, we study the hyperbolicity of (2.11a) and b).

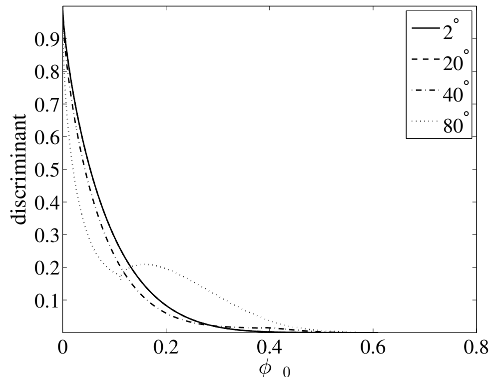

FIGURE 7. Discriminant $\mathcal{D}$ vs. ϕ_0 for different inclination angles α.

2.5. *Hyperbolicity of transport equations*

After switching to f and g, and using (2.11c) and d), the transport problem reads

$$\partial_t h + \partial_x\big(h^3 f(\tfrac{n}{h})\big) = 0$$
$$\partial_t n + \partial_x\big(h^3 g(\tfrac{n}{h})\big) = 0,$$

The Jacobian matrix associated with the above system of conservations laws is

$$h^2 \begin{pmatrix} 3f - \phi_0 f' & f' \\ 3g - \phi_0 g' & g' \end{pmatrix},$$

and the discriminant of the corresponding characteristic polynomial is $\mathcal{D} = h^4 f^2[(3 - \phi_0 f'/f + g'/f)^2 - 12(g/f)']$. Here, the primes denote differentiation with respect to ϕ_0. The hyperbolicity of the transport problem is ensured when $\mathcal{D} \geq 0$. Both the Jacobian matrix and $\mathcal{D}$ are obtained using the intermediate variable $n = \phi_0 h$, where the Jacobian matrix is derived in terms of (h, n) and then rewritten in terms of (h, ϕ_0). This is rather convenient because h may be scaled out of $\mathcal{D}$, and what remains is a condition for hyperbolicity on $f(\phi_0)$, $g(\phi_0)$, and their derivatives with respect to ϕ_0. Figure 7 shows that the discriminant remains strictly positive for all ϕ_0 values within range $\phi_0 \in [0, \phi_\mathrm{m}]$ and all tested values of the inclination angle. We conclude that the system of conservation laws (2.11a) and b) is a well-posed hyperbolic problem for the variables h and n. Next, we examine the parameter dependence of the suspension and particle volume fluxes.

2.6. *Suspension and particle volume fluxes*

The suspension and particle volume fluxes, f and g, are studied next by solving (2.13) numerically for $\tilde{\phi}(s)$ and $\tilde{\sigma}(s)$, and substituting into (2.11c) and d). Fluxes f and g for various values of the inclination angle α are shown in Fig. 8. For small values of α, the suspension volume flux f decreases as ϕ_0 increases due to a corresponding increase in the effective suspension viscosity. Only for large α, f at first increases with ϕ_0 due to to the increase in the corresponding suspension mass and gravitational shear force. For $\phi_0 \to 0$, one recovers the standard lubrication flux, $F = h^3/3$, while for $\phi_0 \to \phi_\mathrm{m}$, the suspension flux tends to zero, $F \to 0$, since $\mu \to \infty$. The particle volume flux g at first increases with ϕ_0 for all α values, due to the increase in the particle content. However, the increase is sublinear since increasing ϕ_0 causes a decrease in the flow velocity $\tilde{u}$, same as for f. Therefore, g must be zero at both $\phi_0 = 0$ and $\phi_0 = \phi_\mathrm{m}$, see Fig. 8b). The transition from the settled regime to the ridged regime occurs when the average particle velocity exceeds

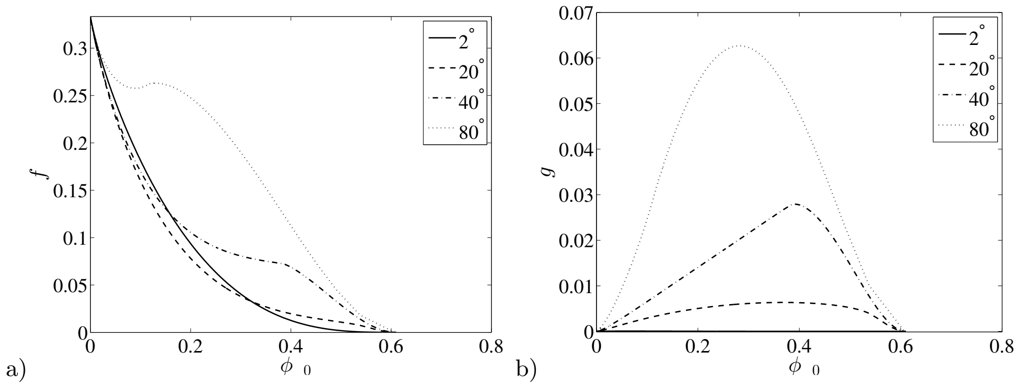

FIGURE 8. Fluxes f in a), and g in b) for different inclination angles α.

the average suspension velocity, i.e. $g/\phi_0 \geq f$, or equivalently when

$$\frac{\int_0^1 \tilde{\phi}\tilde{u}\, ds}{\int_0^1 \tilde{\phi}\, ds} \geq \int_0^1 \tilde{u}\, ds.$$

Since $\tilde{u}$ is an increasing positive function and $\tilde{\phi} > 0$, this transition occurs when $\tilde{\phi}$ changes monotonicity: at $\phi_0 = \tilde{\phi}_{crit}$ given by (2.12).

3. Experiments

We carry out experiments with constant volume particle-laden thin-film flows on an inclined plane. The apparatus we use is identical to the one from Murisic *et al.* (2011). It consists of an acrylic track, $90cm$ long, $14cm$ wide, with $1.5cm$-tall side walls. A gated reservoir with acrylic walls is at the top of the track. Its interior is $14cm$ wide and $10cm$ long; the release gate is manually operated. The collecting tank is at the bottom of the track. The typical thickness of the particle-laden thin films in our experiments is $H \sim \mathcal{O}(1)mm$. The inclination angle of the track, α, may be manually adjusted in the range $5 - 80°$ with precision within a few percent. The suspending liquid we use is PDMS (polydimethylsiloxane, AlfaAesar) with the kinematic viscosity $\nu_\ell = 1000\, cSt$ and density $\rho_\ell = 971\, kg\, m^{-3}$. This PDMS is not cross-linked, and has a relatively low kinematic viscosity and molecular weight. Hence, it is reasonable to assume it behaves as a Newtonian fluid, see e.g. Currie & Smith (1950). The particles are smooth spherical glass beads (Ceroglass) with $\rho_p = 2475\, kg\, m^{-3}$ and mean diameter $d \approx 360\mu m$ (range $300 - 425\mu m$; standard deviation $< 10\%$). This particular particle size is used in order to fulfill the requirement $\varepsilon \ll (d/H)^2 \ll 1$ from §2. Smaller particles may fail to satisfy the equilibrium condition, while larger ones may make the continuum assumption questionable. The equilibrium part of this condition is unlikely to hold for very early times when the film is thick and the suspension is well-mixed, see discussion below. The continuum portion is violated for late times when the suspension becomes very thin.

Each experimental run is carried out using $82.5ml$ of suspension released at once from the reservoir. This volume accounts for losses occurring in the suspension preparation: a small amount of suspension remains in the mixing container after pouring and on the reservoir walls after gate release. We assume that the losses do not affect the suspension composition − it remains well-mixed on the time-scale of the losses. The particles are dyed using water-based food coloring to enhance their visibility. The suspensions are prepared by first weighing the two phases separately (ϕ_0 fraction of particles and $1 - \phi_0$

fraction of liquid) and mixing them slowly to prevent entrapment of air bubbles. A uniformly mixed suspension is then poured into the reservoir, the gate is raised and the suspension is allowed to flow down the incline. The suspension remains well-mixed during the short time-interval between pouring into the reservoir and raising the gate. In fact, in all our experiments, the separation of phases occurs only after the suspension front has traveled some distance down the incline. We carry out a large number (>60) of experimental runs. Each run is repeated to confirm the reproducibility of the results. The solid substrate is cleaned before each run to ensure identical wetting properties and minimize the occurrence of the fingering instability that complicates front tracking.

In this study we focus on the *settled* regime. We record the appearance of the two distinct fronts and monitor their subsequent motion, with the clear liquid front moving faster than the particle one. For this purpose we choose the parameter values based on the experimental data from Murisic *et al.* (2011). In particular, we concentrate on small to moderate values of the bulk particle volume fraction and inclination angle: $\phi_0 = 0.2, 0.3, 0.4$ and $\alpha = 5^\circ \ldots 40^\circ$ in 5°-increments. The experimental data consists of videos captured in a 1920×1080-pixel resolution at $25\,fps$ by a camera equipped with a wide-angle lens. The camera is mounted on a tall tripod $\approx 1m$ above the flow and pointing to $\approx 50cm$ below the release gate. The lens surface is roughly parallel to the track surface, allowing us to capture the whole length of the track with minimal distortion. Each flow is recorded starting with the gate release until the clear liquid front reaches the lower end of the track. In our analysis, we focus on the time-interval starting with the first occurrence of the two distinct fronts and ending before the film becomes very thin. Typically, this amounts to $12 - 25min$ of evolution depending on ϕ_0 and α values. The videos are dissected, extracting individual images at a rate of $0.2\,fps$. The image processing is carried out using a specialized code in MATLAB (MathWorks). It identifies the particle and the liquid front in each image, their visibility enhanced by the particle coloring and the brightness variations near the clear liquid contact line. The preparation of the solid substrate also helps as it leads to fairly straight fronts with reduced fingering of the clear liquid front. In each image, the code detects the two curves in the (x, y) plane corresponding to the two fronts. The values x_p and x_ℓ for each image are obtained by averaging along the curves corresponding to particle and liquid fronts respectively; processing a series of images in this manner yields the time-evolution of the front positions $x_p(t)$ and $x_\ell(t)$. This procedure gives reproducible results within $\pm 5\%$. While some fingering of the clear liquid front is inevitable, the averaging approach is sufficient to provide reliable x_ℓ data for the purpose of comparison with the model predictions. We note that the same approach was successfully used for a simpler case of clear liquid films in Huppert (1982). The averaging of the front position was also utilized in the particle-laden case in Ward *et al.* (2009). Numerical simulations in Mata & Bertozzi (2011) provided further evidence that the averaging technique produces extremely reliable results. The analysis of the fingering phenomena requires inclusion of surface tension in the model and is beyond the scope of present work.

A typical evolution is shown in Fig. 9. Initially, a well-mixed suspension moves down the incline, where the equilibrium condition in (2.3) is unlikely to be satisfied. Toward the end of this initial transient, denoted by $t \in [0, t_{\mathrm{trans}}]$, a transition occurs where two distinct fronts form and the clear liquid front moves ahead of the particle front. We find that the duration of the transient regime increases with ϕ_0; it also increases with α. The separation of phases is detectible once the suspension front has moved $15 - 40cm$ down the incline, depending on the α and ϕ_0 values. We have estimated similar distances in §2, using (2.2). The observation regarding the dependence of t_{trans} on α is also in line with condition (2.2): the validity of the equilibrium assumption in our model relies on a

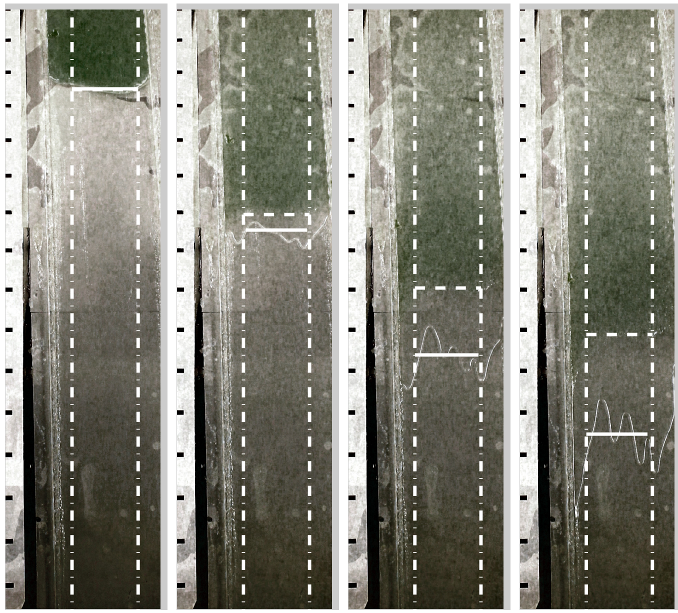

FIGURE 9. Suspension flow for $\phi_0 = 0.3$ and $\alpha = 25°$; time increases from left to right. The white full and dashed lines correspond to the average clear liquid and particle front positions respectively; the black tick-marks on the side of the track are $5cm$ apart; darker regions in the particulate bed indicate higher particle numbers.

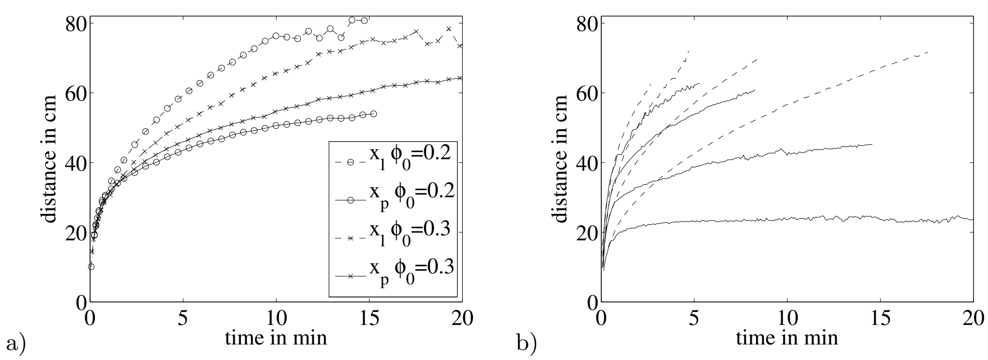

FIGURE 10. Time dependence of the liquid front position, x_ℓ, and the particle front position, x_p, in the experiments with: a) $\phi_0 = (0.2, 0.3)$ and $\alpha = 25°$; and b) $\phi_0 = 0.2$ and $\alpha = (10, 20, 30, 40)°$. In b), full and dashed lines denote x_p and x_ℓ respectively; larger α values result in steeper curves.

similar type of dependence on α, via the $18\rho_\ell \tan\alpha/(\rho_p - \rho_\ell)$ coefficient. We also observe that for small angles, $\alpha < 10°$, the particle front practically comes to a halt, at least on the timescale of our experiments. The increase in the value of α leads to an increase in the ratio of the front positions toward unity: $x_p(t)/x_\ell(t) \to 1$. Naturally, above a critical value of α, defined by (2.12), the flow undergoes a transition toward the ridged regime where the particles move to the contact line of the flow. In our experiments, we stay well away from this transition. While some fingering occurs at the liquid front, no such instability is observed for the particle front. Figure 10 shows the evolution of x_ℓ and x_p for different α and ϕ_0 values.

Two different transients have been identified so far: the one due to the shape of the initial data discussed in connection to the dilute limit and the other, observed in the experiments for early times when the flow is unsteady. In our model, t_{trans} determines the time-instant when the equilibrium assumption in the z-direction becomes valid. The unsteadiness of the flow in experiments may persist beyond the first occurrence of two distinct fronts. Hence, our observations provide a lower bound for t_{trans}. We note that experiments with other particle sizes and suspension volumes may further improve the applicability of the equilibrium assumption. Based on condition (2.2), one may decrease both d and the volume while keeping their ratio fixed. This would shorten the distance traveled by the suspension front during $t \in [0, t_{\mathrm{trans}}]$ without affecting the ratio $(d/H)^2$. However, accurate volume control would be difficult to implement and the fingering instability may also play a more prominent role. The presence of the early-time transient in experiments is actually convenient from the modeling perspective. It provides an opportunity to examine the influence of the shear-induced migration parameters K_c and K_v on the flow, and a way to precisely determine their magnitudes. This would require a comparison between numerical simulations and experiments for $0 < t \leq t_{\mathrm{trans}}$. A more careful study of the transient regime is left for future work. Next, we carry out numerical simulations of (2.11a-e) and (2.13), and compare the model predictions with the experimental data for $t > t_{\mathrm{trans}}$ and different α and ϕ_0 values.

4. Comparison: model predictions vs. experimental data

Equations (2.11a-e) and (2.13) are solved numerically in order to carry out a comparison with the experiments. The equilibrium part (2.13) is solved for intermediate quantities $\tilde{\phi}$ and $\tilde{u}$ using a shooting method with Runge-Kutta; the dynamic transport equations (2.11a-d) are solved for the main variables h and n using an upwind scheme. In this analysis, we only consider the time-interval when our main modeling assumptions hold. Namely, we focus on $t > t_{\mathrm{trans}}$ when two distinct fronts are observable but t is not too large to avoid the film becoming very thin. From the model perspective, this comparison necessitates a non-trivial task of connecting the initial data for the problem, i.e. a well-mixed suspension in the reservoir, with the flow at equilibrium some ~ 10 minutes into the evolution. The benefits of the transient regime for estimation of K_c and K_v values have already been noted in §3.

The initial data for the simulations is obtained as follows. The suspension remains well-mixed during the early-time transient in the experiments, hence we may assume it is of uniform viscosity. The profiles representing a well-mixed suspension at $t = 0$, e.g. $h(0,x) = h_0$ for $-d_x < x < 0$, $h(0,x) = 0$ otherwise, and $n(0,x) = \phi_0 h(0,x)$ are evolved until $t = t_{\mathrm{trans}}$ using the well-known approach from Huppert (1982). Namely, the suspension front moves according to

$$x_{\mathrm{front}}(t) = \left((\rho_\ell + (\rho_p - \rho_\ell)\,\phi_0)\, \frac{9 h_0^2 d_x^2 g \sin\alpha}{\mu(\phi_0)} \right)^{\frac{1}{3}} t^{\frac{1}{3}}.$$

Here, the average concentration in the simulations $0 < \phi_0 < \phi_{\mathrm{m}}$ is adjusted to correspond to each particular experiment and the quantity h_0 is such that the total volume is $h_0\, d_x\, d_y = 82.5\, ml$. The length of the reservoir is $d_x = 10\, cm$ and the width of the track is $d_y = 14\, cm$. In our simulations, we use $x_{\mathrm{front}}(t_{\mathrm{trans}})$ as the initial front position (both liquid and particle). Equations (2.11a-e) and (2.13) govern the subsequent $t > t_{\mathrm{trans}}$ front motion that is compared with the experiments. We note that t_{trans} is estimated experimentally, see §3; our estimate is a lower bound for the true t_{trans} value.

Figure 11 shows a comparison between the model predictions and the experimental

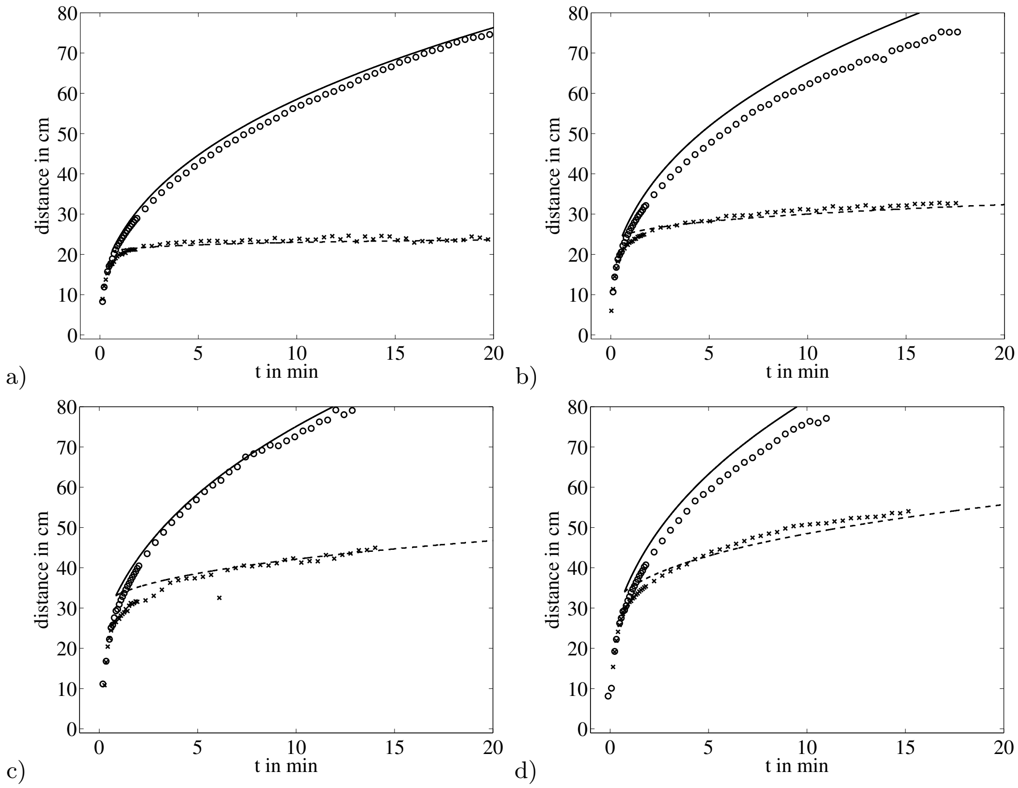

FIGURE 11. Experiment vs. simulation for $t > t_{\text{trans}}$, $\phi_0 = 0.2$ and: a) $\alpha = 10°$; b) $\alpha = 15°$; c) $\alpha = 20°$; and d) $\alpha = 25°$. Model predictions are denoted by lines: full for $x_\ell(t)$ and dashed for $x_p(t)$. Experimental data is denoted by symbols: circles for $x_\ell(t)$ and stars for $x_p(t)$.

data for a fixed average concentration $\phi_0 = 0.2$, and a few different values of the inclination angle, $\alpha = (10, 15, 20, 25)°$. The comparison is carried out for $t_{\text{trans}} < t < 20min$, a time-interval sufficiently long to illustrate the main points while ensuring the validity of the main modeling assumptions. Qualitatively, the model fully captures the experimental observations. The quantitative agreement is also excellent, despite the fact that the initial condition in the simulations overestimates the suspension front position compared to the experiments. The longer the transient, i.e. the larger the inclination angle, the more evident this issue becomes. Nevertheless, the deviation between model predictions and experiments is relatively small for all α values we consider. Figure 12 shows equivalent results for $\phi_0 = 0.3$. The agreement is remarkable, keeping in mind that K_c and K_v have not been fitted to improve on these predictions. The overestimation in the initial conditions for the simulations contributes to a slight quantitative mismatch between model and experiments. Finally, Fig. 13 compares the results for $\phi_0 = 0.4$. The agreement is still fairly good, but the overestimation in the initial conditions is now quite pronounced. This may be related to the fact that here t_{trans} is larger than at $\phi_0 = 0.2$ or 0.3; the connection between ϕ_0 and t_{trans} has already been noted in §3.

The overestimation of the front positions used as the initial data for the simulations may result due to several factors. The first is connected to the presence of the transient in the experiments, and the fact that its duration and the associated length-scale in (2.2) are estimated roughly. The second is due to our use of the Huppert solution, possibly a rather crude approach, to evolve the well-mixed initial data from $t = 0$ until $t = t_{\text{trans}}$. Finally,

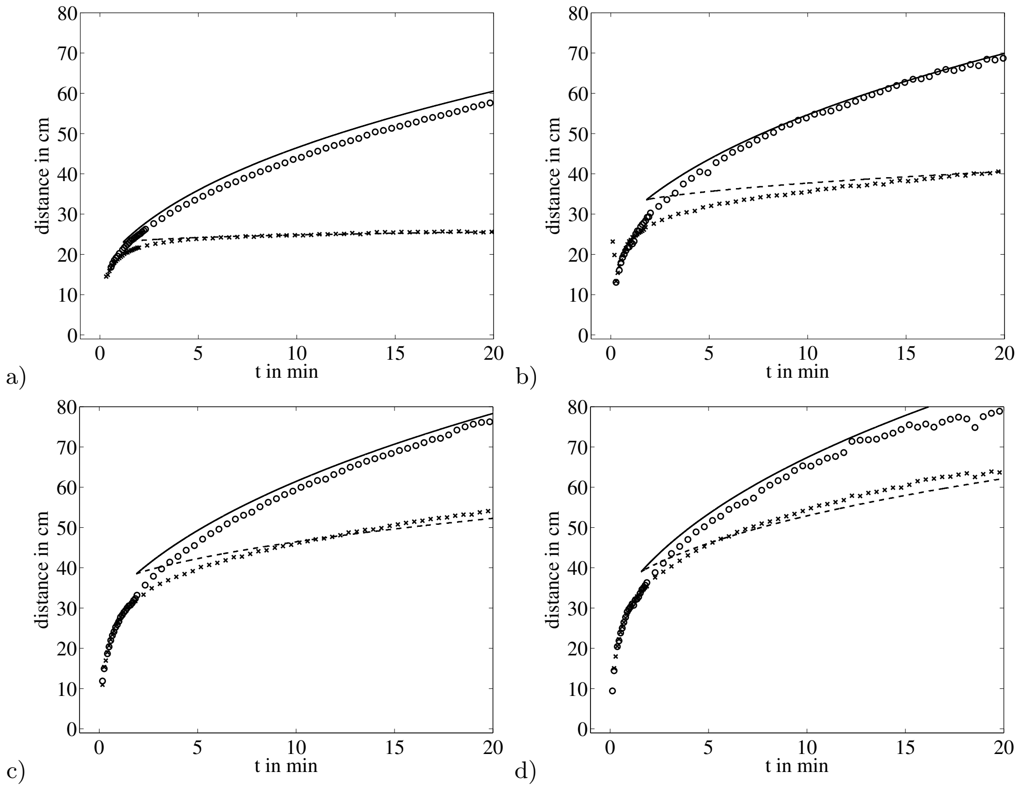

FIGURE 12. Experiment vs. simulation for $t > t_{\text{trans}}$, $\phi_0 = 0.3$ and: a) $\alpha = 10°$; b) $\alpha = 15°$; c) $\alpha = 20°$; and d) $\alpha = 25°$. Simulations: full line for $x_\ell(t)$, dashed line for $x_p(t)$; experiments: circles for $x_\ell(t)$, stars for $x_p(t)$.

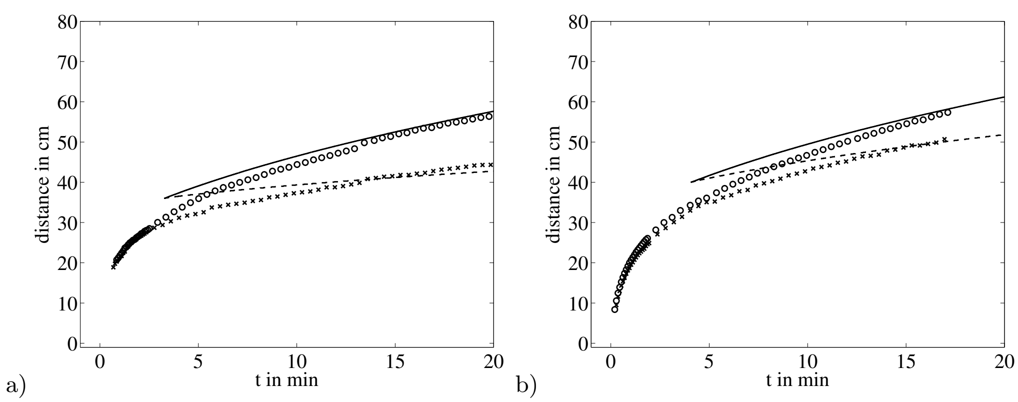

FIGURE 13. Experiment vs. simulation for $t > t_{\text{trans}}$ and $\phi_0 = 0.4$: a) $\alpha = 15°$; b) $\alpha = 20°$. Lines are simulations : full for $x_\ell(t)$, dashed for $x_p(t)$; experiments: circles for $x_\ell(t)$, stars for $x_p(t)$.

there is also the transient due to the shape of the initial data, identified in our discussion of the dilute approximation. Imprecise knowledge of the initial data fed into the Huppert solution affects the outcome even outside the dilute limit. Despite the combined effect of these factors on the outcome of the comparison, the agreement between model predictions and experiments in Figs. 11, 12 and 13 is still quite remarkable. Further analysis of the transient stage including experiments and numerical simulations would further improve these results. We note that for denser suspensions other factors, e.g. the validity of the employed viscosity law, may also be relevant.

5. Conclusions

In this paper, we focus on the *settled* regime observed in particle-laden thin-film flows on an incline. In this regime, particles settle to the solid substrate and the clear liquid film flows over the sediment. The slower particle and the faster clear liquid front form.

We first derive a continuum model, starting with the Stokes' equations for the suspension and a transport equation for the particles. We assume that the suspension behaves like a Newtonian fluid. The particle model relies on the diffusive flux phenomenology, and it includes the effects of shear-induced migration and hindered settling due to gravity. We apply the lubrication-style scales and carry out an asymptotic analysis of the resulting equations. Our main assumption is that the particle distribution in the z-direction is in equilibrium, i.e. the corresponding dynamics occur on a rapid time-scale so that the steady-state is quickly established and the total particle flux in the z-direction is zero. Hence, we are able to reconstruct the z-profiles for the particle volume fraction and the suspension velocity. Our asymptotics approach allows us to connect the leading order equilibrium model to the slow dynamics of particle and suspension transport down the incline. We focus on the averaged quantities, the film thickness and the particle number, which obey a coupled system of advection equations – a pair of hyperbolic conservation laws – thereby closing the approximation and completing the theoretical framework.

The derived model is general as it allows the use of different effective suspension viscosity relations and different parameter values related to the particle flux. We compare different viscosity/parameter combinations from literature and study the sensitivity of model predictions. We find that all considered combinations predict similar particle volume fraction profiles. On the other hand, the velocity and fluxes predictions are substantially affected by the details of the viscosity law that is used. With the exception of Einstein's linear viscosity law that is not applicable for dense suspensions by definition, all others give comparable predictions. The combination from Murisic *et al.* (2011) that was already successful in modeling particle-laden thin-film flows is chosen for further analysis. We first consider the dilute limit for which we derive an analytic solution and discuss the early-time transient due to the shape of the initial data. The exact solution for the dilute approximation also reveals the two front configuration, where the clear liquid front is faster than the particle one, typical for the settled regime. The hyperbolicity of the transport equations is also confirmed.

Next, we carry out experiments using fixed volume suspensions, consisting of glass beads and PDMS. We vary the bulk particle volume fraction and the inclination angle of the solid substrate within the permitted range for the settled regime. Our experimental setup allows us to detect the particle and the clear liquid fronts, and precisely monitor their motion down the incline. We also detect another transient for $0 < t \leq t_{\mathrm{trans}}$ where the mixture remains well-mixed, and estimate t_{trans}. We proceed by computing numerical solutions for our model, and comparing the model predictions for the particle and the clear liquid front motion with the experiments. This is carried out for $t > t_{\mathrm{trans}}$, when the equilibrium assumption in the vertical direction is valid. We find excellent agreement between model and experiments, in both qualitative and quantitative sense, especially for lower values of the average particle volume fraction.

In order to improve the model, a detailed investigation of the transient phase is required, including experiments and a theoretical approach. An important question is how early the equilibrium in the z-direction may be assumed. We hope that our results will motivate future experiments where the steadiness of the flow will be examined and accurate measurements of the transient time t_{trans} will be carried out. The inclusion of surface tension may also be needed in order to model the transient phase. We anticipate that numerical simulations will eventually provide full access to the well-mixed transient. The presence of the transient in experiments may also be useful for studying the influence of the shear-induced migration parameters on the flow and precise determination of their magnitudes. For this purpose one may consider either an asymptotic reduction of our model appropriate for the transient regime or direct numerical simulations. Another interesting question is the validity of the employed hindrance model and $\mu(\tilde{\phi})$ formulation for denser suspensions. Future work should also include higher order terms in the dynamic equations, corresponding to the capillary and normal gravitational forces. This would allow for a comprehensive study of the different settling regimes, the evolution of the contact line region, and the details of the fingering instability.

Acknowledgement

This work was supported by NSF grant DMS-1048840 and UC Lab Fees Research Grant 09-LR-04-116741-BERA. DP acknowledges support by DFG MATHEON C10.

REFERENCES

Acrivos, A., Batchelor, G.K., Hinch, E.J., Koch, D.L. & Mauri, R. 1992 Longitudinal shear-induced diffusion of spheres in a dilute suspension. *Journal of Fluid Mechanics* **240**, 651.

Batchelor, G. K. 1972 Sedimentation in a dilute suspension of spheres. *J.Fluid Mech.* **52**, 245.

Brady, J. F. & Morris, J. F. 1997 Microstructure of strongly sheared suspensions and its impact on rheology and diffusion. *J.Fluid Mech.* **348**, 103.

Cook, B. P. 2008 Theory for particle settling and shear-induced migration in thin-film liquid flow. *Phys. Rev. E* **78**, 045303.

Cook, B. P., Bertozzi, A. L. & Hosoi, A. E. 2007 Shock solutions for particle-laden thin films. *SIAM J.Appl. Math.* **68**, 760.

Currie, C.C. & Smith, B.F. 1950 Flow characteristics of organopolysiloxan fluids and greases. *Ind. Eng. Chem.* **42**, 2457.

Davis, R. H. & Acrivos, A. 1985 Sedimentation of noncolloidal particles at low Reynolds-numbers. *Ann. Rev. Fluid Mech.* **17**, 91.

Eilers, V.H. 1941 Die Viskosität von Emulsionen hochviskoser Stoffe als Funktion der Konzentration. *Kolloid* **97**, 313.

Einstein, A. 1906 Eine neue Bestimmung der Moleküldimensionen. *Annalen der Physik* **19**, 289.

Einstein, A. 1911 Berichtigung zu meiner Arbeit: "Eine neue Bestimmung der Moleküldimensionen". *Annalen der Physik* **34**, 591.

Ferrini, F., Ercolani, D., de Cindio, B., Nicodemo, L., Nicolais, L. & Renaudo, S. 1979 Shear viscosity of settling suspensions. *Rheologica Acta* **18**, 289.

Grunewald, N., Levy, R., Mata, M., Ward, T. & Bertozzi, A.L. 2010 Self-similarity in particle-laden flows at constant volume. *Journal of Engineering Mathematics* **66** (1), 53.

Huppert, H. 1982 Flow and instability of a viscous current down a slope. *Nature* **300**, 427.

Krieger, I.M. & Dougherty, T.J. 1959 A mechanism for non-Newtonian flow in suspensions of rigid spheres. *Trans. Soc. Rheol.* **3**, 137.

Kynch, G.J. 1952 A theory of sedimentation. *Transactions of the Faraday society* **48**, 166.

Leighton, D. & Acrivos, A. 1987*a* Measurement of shear-induced self-diffusion in concentrated suspensions of spheres. *J.Fluid Mech.* **177**, 109.

Leighton, D. & Acrivos, A. 1987*b* The shear-induced migration of particles in concentrated suspensions. *J.Fluid Mech.* **181**, 415.

Maron, S.H. & Pierce, P.E. 1956 Application of Ree-Eyering generalized flow theory to suspensions of spherical particles. *J. Colloid Sci.* **11**, 80.

Mata, M.R. & Bertozzi, A.L. 2011 A numerical scheme for particle-laden thin film flow in two dimensions. *J. Comput. Phys.* **230**, 6334.

McGeary, R.K. 1961 Mechanical packing of spherical particles. *J. Am. Ceram. Soc.* **44**, 513.

Merhi, D., Lemaire, E., Bossis, G. & Moukalled, F. 2005 Particle migration in a concentrated suspension flowing between rotating parallel plates: investigation of diffusion flux coefficients. *J. Rheol.* **49**, 1429.

Morris, J. F. & Boulay, F. 1999 Curvilinear flows of noncolloidal suspensions: The role of normal stresses. *J.Rheology* **43**, 1213.

Morris, J. F. & Brady, J. F. 1998 Pressure-driven flow of a suspension: buoyancy effects. *Int. J.Multiphase Flow* **24**, 105.

Murisic, N., Ho, J., Hu, V., Latterman, P., Koch, T., Lin, K., Mata, M. & Bertozzi, A.L. 2011 Particle-laden viscous thin-film flows on an incline: Experiments compared with a theory based on shear-induced migration and particle settling. *Physica D: Nonlinear Phenomena* **240**, 1661.

Nott, P. R. & Brady, J. F. 1994 Pressure-driven flow of suspensions - simulation and theory. *J.Fluid Mech.* **275**, 157.

Onoda, G.Y. & Liniger, E.G. 1990 Random loose packings of uniform spheres and the dilatancy onset. *Phys. Rev. Lett.* **64**, 2727.

Oron, A., Davis, S.H. & Bankoff, S.G. 1997 Long-scale evolution of thin liquid films. *Reviews of Modern Physics* **69** (3), 931.

Phillips, R. J., Armstrong, R. C., Brown, R. A., Graham, A. L. & Abbott, J. R. 1992 A constitutive equation for concentrated suspensions that accounts for shear-induced particle migration. *Phys. Fluids A* **4**, 30.

Richardson, J. F. & Zaki, W. N. 1954 The sedimentation of a suspension of uniform spheres under conditions of viscous flow. *Chem. Eng. Sci.* **3**, 65.

Schaflinger, U., Acrivos, A. & Zhang, K. 1990 Viscous resuspension of a sediment within a laminar and stratified flow. *Int. J.Multiphase Flow* **16**, 567.

Stickel, J.J. & Powell, R.L. 2005 Fluid mechanics and rheology of dense suspensions. *Ann. Rev. Fluid Mech.* **37**, 129.

Timberlake, B. D. & Morris, J. F. 2005 Particle migration and free-surface topography in inclined plane flow of a suspension. *J.Fluid Mech.* **538**, 309.

Torquato, S., Truskett, T.M. & DeBenedetti, P.G. 2000 Is random close packing of spheres well defined? *Phys. Rev. Lett.* **84**, 2064.

Ward, T., Wey, C., Glidden, R., Hosoi, A. E. & Bertozzi, A. L. 2009 Experimental study of gravitation effects in the flow of a particle-laden thin film on an inclined plane. *Phys. Fluids* **21**, 083305.

Zhang, K. & Acrivos, A. 1994 Viscous resuspension in fully developed laminar pipe flows. *Int. J.Multiphase Flow* **20**, 579.

Zhou, J. J., Dupuy, B., Bertozzi, A. L. & Hosoi, A. E. 2005 Theory for shock dynamics in particle-laden thin films. *Phys. Rev. Lett.* **94**, 117803.